Investigation of Noise Sources in Three-Stream Jets using Turbulence Characteristics

Marcie Alberta Stuber

Thesis submitted to the faculty of the Virginia Polytechnic Institute and State University in partial fulfillment of the requirements for the degree of

Master of Science
In
Aerospace Engineering

K. Todd Lowe, Co-Chair
Wing F. Ng, Co-Chair
William J. Devenport

February 13, 2017
Blacksburg, Virginia

Keywords: jet noise, jet noise reduction, three-stream nozzles, eddy convection velocity

Investigation of Noise Sources in Three-Stream Jets using Turbulence Characteristics

Marcie Alberta Stuber

ACADEMNIC ABSTRACT

Key areas of noise sources are investigated through comparison of eddy convection velocity and turbulence measurements in three-stream nozzles. A Time-Resolved Doppler Global Velocimetry (TR-DGV) Instrument was applied to the Nozzle Acoustic Test Rig (NATR) at NASA's Aero-Acoustic Propulsion Lab (AAPL) to measure convection velocity. Particle image velocimetry (PIV) measurements provided mean velocity and turbulence intensity. Eddy convection velocity results were obtained from the TR-DGV data for three-stream nozzle configurations using a cross-correlation approach. The three-stream cases included an axisymmetric and an asymmetric nozzle configuration. Results of the VT TR-DGV convection velocity were compared to NASA PIV mean and turbulence intensity data. For the axisymmetric case, areas of high convection velocity and turbulence intensity were found to be from 4 to 6 diameters downstream. Comparison of convection velocity between the axisymmetric and offset case show this same region as the greatest reduction in convection velocity due to the offset. These findings suggest this region along the centerline near the end of the potential core is an important area for noise generation with jets and contribute to the noise reductions seen from three stream offset nozzles. An analysis of a one-dimensional wavepacket model was completed to provide understanding of the effect of the various convection velocities seen in the flow. Comparison of a wavepacket with a convection velocity of $0.6U_j$ to a wavepacket with a convection velocity of $0.8U_j$ showed that an increase in convection velocity shifts the wavenumber spectrum to higher wavenumbers as expected. It was also observed that for the higher convection velocity wavepacket, higher frequencies are more acoustically efficient, while mid frequencies are the most efficient radiators in the lower convection velocity case. Using mean velocity, turbulence intensity, and convection velocity areas of likely to generate noise are identified and possible fundamental mechanisms responsible for the noise generation are discussed.

Investigation of Noise Sources in Three-Stream Jets using Turbulence Characteristics

Marcie Alberta Stuber

GENERAL AUDIENCE ABSTRACT

Noise from the jet exhaust plumes of aircraft engines continues to be a problem in the aerospace field, specifically for applications where high speeds and temperatures are required. This study works to identifity the noise producing areas in a high speed, heated jet plume for a new type of exhaust nozzle configurations. Identification of the noise producing regions will allow desing of quieter aircraft engines. Traditionally, there are two streams in the exhaust of aircraft engines. This research is a study of a new exhaust nozzle configuration with an additional third exhaust stream. Specifically, two three-stream nozzle configurations are studied: one that is symmetric and one with the third stream shifted relative to the other exhast streams which is called the offset configuration. Past studies have shown that three stream jets and offset three stream jets offer noise reductions. Of the two configurations studied, the offset configuration offers greater potential for noise reduction. The flow field of three stream jet and a three stream shifted jet are analyzed. Flow properites relating to the speed of the jet, the level of turbulence, and the speed at which flow structures convect are analyzed for the symmetric three stream nozzle. The region along the jet centerline is identified as a likely noise producing area based on analysis of the flow properties. Comparison of the three stream symmetric configuration with the three stream offset configuration shows the offset configuration reduces the convection speed of structure along the jet centerline. This reduction in convection velocity is an explanation for the noise reduction caused by the offset nozzle configuration. A simple mathematical model to describe how the flow structures convect is developed in order to better understand how the differenct convection speeds observed impact noise production. Many researchers in the past have suggested that the area of high shearing caused by the velocity difference between the jet and the surrounding is the dominant noise producing region, however, analysis of the experiemental results from this research has found the centerline region as a likely noise producing region. Results from the model, therefore, were obtained for both the high shearing region and the centerline region previously identified for both jet configurations. It was found that the region along the centerline showed a greater difference in likeliness to produce noise, further suggesting that the reigon along the centerline is important for noise production.

Acknowledgements

I would like to thank the many people who have helped and supported me throughout my research. First, I would like to thank my co-advisors, Dr. Lowe and Dr. Ng. Their support and guidance throughout my graduate studies that helped me become the engineer that I am today. A special thanks to the other member of my advisory committee, Dr. Devenport, for his insight in this work.

I would like to acknowledge Dr. Tobias Ecker. This research would not have been possible with his hard work in collecting the TR-DGV data that was analyzed in this thesis. Additionally, I would like to acknowledge Drs. Brenda Henderson and Mark Wernet of the NASA Glenn Research Center for providing the PIV results that were crucial to the analysis done in the thesis. I would also like to thank Dr. Brenda Henderson for providing insights through multiple discussions.

I would also like to acknowledge the Office of Naval Research (ONR). This work is sponsored by Navy grants N00014-16-1-2444 and N00014-14-1-2836, which is funded by the Office of Naval Research and managed by Dr. Knox Millsaps.

I would like to thank the support that my research group and the CREATe center has given me while at Virginia Tech. They have offered me day to day guidance and advice, and I will be forever grateful for their friendship. Special thanks to Dan Cadel, Kara Crosser, Kyle Daniel, Will George, Tamy and Pedro Guimarães, Liselle Joseph, Anthony Millican, Nick Molinaro, Eric Rolfe, Sean Shea, Tyler Vincent, and Chi Young Moon.

Finally, I would like to thank my family and my fiancé for their constant support throughout my graduate studies.

Table of Contents

List of Figures

List of Tables

Nomenclature

a	Speed of sound in the jet at the nozzle exit plane
a_1	Speed of sound in faster moving stream
a_2	Speed of sound in slower moving stream
a_∞	Speed of sound in the ambient medium
D	Diameter of jet at nozzle exit
D_{eqA}	Equivalent diameter based on the total area of the nozzle
D_{eqC}	Equivalent diameter based on the area of the core
f	Time frequency
G_{ii}	Wavenumber spectrum
k	Wavenumber
k_0	Initial wavenumber
k_a	Wavenumber that divides radiating and non-radiating components
l	Characteristic length of wavepacket
M_c	Acoustic eddy convection Mach number
$M_{c\,sym}$	Symmetric Convection Mach number
M_j	Isentropic Mach number
p	Pressure in the jet
p_a	Atmospheric static pressure
p_0	Total pressure
R	Gas constant
Re	Reynolds number
R_{ij}	Cross-correlation coefficient
r	Radial location
S	Function for the shape of the wavepacket
SNR	Signal to noise ratio
St	Strouhal number
s	Generic mean subtracted flow fluctuation variable
T	Data acquisition time period
T_0	Total temperature of exiting fluid

$\boldsymbol{T_{ij}}$	Lighthill stress tensor
$\boldsymbol{T_s}$	Static temperature of exiting fluid
$\boldsymbol{t}$	Time
$\boldsymbol{U}$	Mean axial velocity
$\boldsymbol{U_1}$	Velocity of faster moving stream
$\boldsymbol{U_2}$	Velocity of slower moving stream
$\boldsymbol{U_c}$	Axial eddy convection velocity
$\boldsymbol{U_j}$	Isentropic exit velocity
$\boldsymbol{u}$	Fluctuation velocity
$\boldsymbol{u'}$	Axial turbulence intensity (standard deviation)
$\boldsymbol{x}$	Axial location
$\boldsymbol{x_0}$	Initial axial location
$\boldsymbol{\gamma}$	Specific heat ratio
$\boldsymbol{\Delta x}$	Physical sensor spacing
$\boldsymbol{\delta_{ij}}$	Kronecker delta
$\boldsymbol{\delta U_c}$	Uncertainty in convection velocity calculation
$\boldsymbol{\delta \Delta x}$	Uncertainty in sensor spacing
$\boldsymbol{\delta \tau}$	Uncertainty in correlation lag time
ς	Correlation axial spacing
ς_r	Correlation axial spacing on convective ridge
$\boldsymbol{\theta}$	Angle relative to jet axis
$\boldsymbol{\mu}$	Dynamic Viscosity
$\boldsymbol{\xi}$	Correlation radial spacing
$\boldsymbol{\rho}$	Density in the exiting fluid
$\boldsymbol{\sigma^2_{deterministic}}$	Variance of the deterministic content of the signal
$\boldsymbol{\sigma^2_{random}}$	Variance of the random content of the signal
$\boldsymbol{\tau}$	Correlation lag time
$\boldsymbol{\tau_{ij}}$	Viscosity tensor
$\boldsymbol{\tau_r}$	Correlation lag time on convective ridge
$\boldsymbol{\omega}$	Radian frequency

1. Introduction

Noise from supersonic jet plumes has been a problem in the aviation industry since the introduction of aircraft engines [1]. Although advances have been made in the reduction of jet noise, these advances have primarily been for transonic and subsonic commercial applications. Renewed interest in supersonic transport vehicles through the Commercial Supersonic Technology (CST) project of the Advanced Air Vehicles Program (AAVP) at NASA has prompted research in mitigating jet noise in heated, high speed jet plumes [2]. Based on the set performance and noise goals of the program, new engine technologies are being researched. One of the more promising ideas is a variable cycle or adaptive cycle engine which would all for a third exhaust stream, in addition to the bypass and core streams that are already commonplace in aircraft engines [2]. Recent computational and experimental work has shown that nozzles with a tertiary stream offer a potential for noise reduction [2, 3]. Additional studies have shown that asymmetry in jet plumes reduced jet noise on the locally thick side [4, 5, 6]. The asymmetry was introduced by offsetting a secondary or tertiary stream in the radial direction.

Research on heated, high speed jet noise is also of interest to the Navy. Due to the stricter performance and size requirements of military tactical engines, significant advances have not been made for jet noise from military tactical engines. The US Department of Veterans Affairs (VA) spends over $1 billion each year on hearing loss claims, with 28% of those from the Navy [8]. In the past, to protect service persons from hearing loss due to jet noise, the Navy put significant effort into improving hearing protection for service persons. While advances in hearing protection have been made, with advanced designs offering protection up to 47 dB, noise levels for those working in close proximity to aircraft can exceed 140 dB [9]. New efforts have now been made by the Navy to better understand the fundamental mechanisms causing noise in jet plumes at conditions seen in military aircraft engines.

Overall, a better understanding of the physics producing jet noise can lead to better engine design with reduced jet noise. Further, continued research on techniques to reduce noise, such as the use of a third stream, is vital to address the jet noise problem in both supersonic transport vehicles and military tactical aircraft.

Papamoschou et al. [10] have shown that a component of supersonic jet noise, the radiation efficiency, is a function of the acoustic convection Mach number of the turbulent eddies in the jet.

The acoustic eddy convection Mach number is defined as, U_c/a_∞, the eddy convection velocity divided by the ambient speed of sound. The radiation efficiency is therefore a function of the eddy convection velocity of the turbulent structures in the jet. Past computational work by Papamoschou et al. [10] has also shown that radiation efficiency scales non-linearly with the eddy acoustic convection Mach number. Due to the non-linearity, a reduction in the acoustic eddy convection Mach number is the most effective method for reducing jet noise. Measuring eddy convection velocity in jets, therefore, will provide insight into the mechanisms for reducing noise in heated, three-stream axisymmetric and offset jet streams which have been devised based upon the hypothesis that they reduce convection velocity.

To measure eddy convection velocity a Time-Resolved Doppler Global Velocimetry (TR-DGV) instrument was applied to heated three-stream axisymmetric and asymmetric offset nozzle configurations at the NASA Aero-Acoustic Propulsion Lab (AAPL) located at Glenn Research Center [11]. The current work aims to better understand the fundamental physics which cause tertiary streams and offset streams to reduce jet noise. It will be shown that comparison of eddy convection velocity and flow characteristics obtained using two component PIV allows identification of key areas in the flow responsible for noise generation. Investigation of differences between convection velocity in the axisymmetric and asymmetric configurations will reveal differences which contribute to the noise reduction in the offset configuration. Defining these areas improves nozzle designs by targeting regions that will be most efficient in reducing jet noise. In addition to experimental studies, an analytical one-dimensional wavepacket model is developed to provide insights in regard to the effect of convection velocity on radiated noise. This work presents the combined analysis of experimentally measured turbulence characteristics and the evaluation of a basic wavepacket model to provide a better understanding of the mechanisms causing noise generation in heated three-stream jets.

1.1. Overview

This thesis is divided into six chapters and an appendix. The first chapter describes the motivation for a better understanding of the noise sources in heat, high speed three stream jets, which is the subject of the current work. Chapter 2 provides an overview of free, single and mutli-stream jets, along with a review of relevant jet noise literature. The characteristic features and properties of single and multi-stream jets are described along with a review of jet noise topics such

as classical acoustic analogies, the determination of the radiating components of jet noise, and the importance of large scale structures in jet noise. Chapter 3 provides a review of correlations measurements in jet noise research. Correlations measurements for noise source identification and convection velocity calculation are reviewed. Chapter 4 describes the methods used for collecting and processing the convection velocity data. In addition, a description of the wavepacket model used to better understand the effect of convection is given along with assumptions made for this model. Chapter 5 details the results for the VT TR-DGV convection velocity for both the axisymmetric and the offset configurations and the comparison with the NASA PIV mean and turbulence intensity data. Results for the wavepacket model are also discussed in this chapter. Chapter 6 summarized the conclusions of the current work.

2. Background and Review of Relevant Literature

The following section provides background information and a review of literature relevant to the author's work. Section 2.1 gives a background on free jets including the structure of free jets along with a discussion on how characteristic properties are defined and calculated. A background of jet noise theory is discussed in Section 2.2 followed by a review of multi-stream jets in Section 2.3.

2.1. Overview of Free Jets

A free jet consists of a fluid exhausting from a nozzle into the surrounding medium. A diagram of a simple, single stream, free jet is shown in Figure 2.1. The surrounding medium can be at rest (as is the case for many laboratory and field experiments) or the surrounding medium may be moving relative to the jet (as is the case for the exhaust of aircraft engines when in flight). An initial region called the potential core exists just beyond the nozzle exit. In this region the turbulence is low, and the velocity of the fluid is close to the velocity at which the fluid exits the nozzle. A shear layer develops between the fluids moving at different velocities. The shear layer is dominated by instabilities in the form of turbulent eddies, which develop between the faster moving fluid and the surrounding medium. The turbulent eddies entrain the slower surrounding medium, and the shear layer grows as the eddies convect downstream. Eventually, the shear layer grows large enough that it interacts across the opposite sides of the jet. The potential core ends at

which point the shear layer region overcomes the potential core region. The jet plume then enters an adjustment region and eventually reaches the fully developed region [12]. The length of the potential core is affected by both the Mach number and temperature of the jet. An increase in the Mach number results in an increase in the potential core length, while an increase in the temperature results in a reduction in the potential core length [10, 11]. For jet noise, the primary regions of interest in jets are the initial developing shear layer before the potential core ends and the region immediately downstream of the potential core [12]. These regions extend approximately a distance of four to ten jet diameters downstream of the nozzle exit plane. For simplification the terms free jet and jet will be used interchangeably in this work.

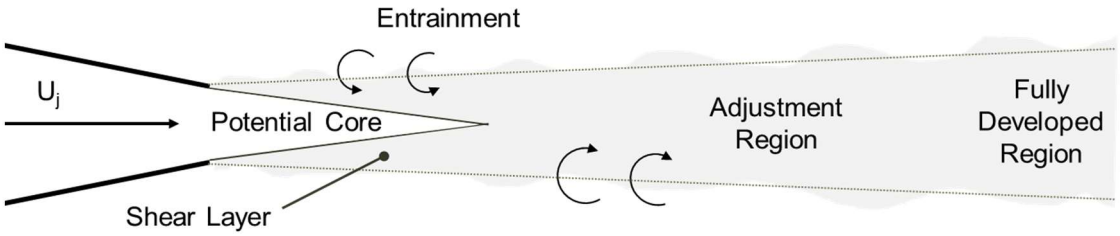

Figure 2.1. Diagram of single stream free jet

The growth of the shear layer was studied by Brown and Roshko [15] to understand the effects of density on the spreading rate. It was found that the overall compressibility of the jet had a greater effect on the change in spreading rate of the shear layer compared to the density ratio of the two mixing fluids. In addition, a measure of the compressibility was found to be the symmetric convection Mach number calculated using Equation (2.1),

$$M_{c\,sym} = \frac{U_1 - U_2}{a_1 + a_2} \tag{2.1}$$

where the subscripts one and two denote the faster moving fluid and the slower moving fluid, respectively. For single stream jets, the slower moving fluid may be the ambient surrounding so U_2 may be zero.

2.1.1. Characteristic Properties of Free Jets

The characteristic velocity of the jet used for normalization is the isentropic exit velocity which is found using the isentropic relations. In many cases, the isentropic relation using the ratio of the total pressure to the static pressure is used to calculate the isentropic exit velocity. For a

subsonic or ideally expanded supersonic jet, the static pressure of the exiting fluid is the same as the pressure of the surrounding fluid which simplifies the isentropic relation shown in Equation (2.2).

$$\frac{p_0}{p_a} = \left(1 + \frac{\gamma - 1}{2} M_j^2\right)^{\frac{\gamma}{\gamma - 1}} \tag{2.2}$$

The isentropic Mach number is determined from Equation (2.2) for a given pressure ratio. The isentropic exit velocity is calculated using the definition for Mach number given by Equation (2.3).

$$M_j = U_j / a \tag{2.3}$$

The definition requires the local speed of sound in the exiting fluid, since the speed of sound in the fluid may be different from the surrounding medium due to differences in temperature. The local speed of sound is calculated using Equation (2.4).

$$a = \sqrt{\gamma R T_s} \tag{2.4}$$

The characteristic dimension for the flow is the jet diameter, and dimensions are commonly given in terms of the jet diameter.

A common parameter used to define the flow from a jet is the Reynolds number. The Reynolds number is a ratio of the inertial forces of the flow to the viscous forces in the flow, and is found through the definition given in Equation (2.5).

$$Re = \frac{\rho U_j D}{\mu} \tag{2.5}$$

The density of the flow is found using the ideal gas law given in Equation (2.6),

$$p_a = \rho R T_s \tag{2.6}$$

and the dynamic viscosity is found using Sutherland's relation assuming that it is only a function of temperature [16].

2.2. Jet Noise Fundamentals

In the study of jet noise three physically distinct regions exist: the acoustic far field, the near field, and the vortical turbulent region. The region of the jet itself is the vertical, turbulent region and is dominated by hydrodynamic pressure fluctuations [17]. The region far from the jet is termed

the acoustic far field. In this region only acoustic waves are present which are described by the wave equation [18]. The region between the jet and the acoustic far field is called the near field. In this region fluctuations from both hydrodynamic fluctuations and acoustic sound waves are significant. The hydrodynamic fluctuations are from the turbulence of the adjacent jet, while the acoustic sound waves are the beginning of the acoustic field [17].

Noise from jets is composed of three components, screech tones, broadband shock noise, and turbulent mixing noise [19]. Noise due to screech almost entirely radiates in the upstream direction [19]. Screech tones are primarily observed in supersonic, cold jets operated at over-expanded conditions and is found to decrease in intensity with increasing temperature [20]. Broadband shock noise is generated due to shock cell structures in supersonic jet plumes. The shock cell structures are formed due to flaws in the nozzle geometry and/or operating the nozzle at off design conditions [20]. Turbulent mixing noise is generated by the turbulence in the shear layers of the jet. A defining characteristic of turbulence is the cascade of length scales ranging from the smallest Kolmogorov scales to the largest energy containing region [21]. For turbulent mixing noise the scales are loosely separated into fine scale and large scale turbulence; the fine scale turbulence is considered the mechanism generating background noise while the large scale turbulence is considered the dominant noise source [19]. The noise from jets have a dominant noise direction which for high speed jets is downstream in directions at small polar angles from the jet axis.

A jet is defined as supersonic if the fluid is moving faster than the speed of sound in the fluid. For the current work the flow is heated and is not supersonic with respect to the speed of sound within the jet, so screech and broadband shock noise are not of interest for this study. The focus will be on turbulent mixing noise. A discussion of relevant literature for turbulent mixing noise theory is found in the following subsections.

2.2.1. Classical Jet Noise Theory

Lighthill [22] developed his acoustic analogy in 1952 with the goal to relate properties of the jet flow to acoustic properties. While flow physics are governed by the Navier-Stokes equations, the acoustic properties of the flow are governed by the wave equation. Lighthill was able to relate the flow physics to the acoustic through recasting the Navier-Stokes equations in terms of the wave equation. In doing so, Lighthill was able to identify the sources of jet noise, as any terms that were

not part of the linear wave propagation equation. The resulting source was termed the Lighthill stress tensor, and is given in Equation (2.7).

$$T_{ij} = \rho u_i u_j + (p - \rho a_\infty^2)\delta_{ij} - \tau_{ij} \tag{2.7}$$

Based on this analogy the noise sources are due to differences in stresses in the flow itself, both Reynolds stresses and stresses due to pressure and viscosity, and those in the acoustic field. The acoustic field is defined as the region around the jet which does not contain the hydrodynamic, turbulent fluctuations of the jet, and is often called the ambient medium. Lighthill [23] further hypothesized that all stresses except those due to the Reynolds stresses, $\rho u_i u_j$, are negligible.

In order to make the acoustic analogy Lighthill assumed that the flow was moving slow relative to the surrounding medium; however, as many flows of engineering interest are moving much faster the acoustic analogy needed to be corrected. Although Lightill recognized the importance of convection in his theory, Ffowcs-Williams [24] improved the acoustic analogy to better take into account the effects of convection and showed that the acoustic intensity should be modified by the factor given in Equation (2.8),

$$(1 - M_c \cos(\theta))^{-5} \tag{2.8}$$

where θ is the angle to the jet axis. This factor is often called the convection amplification factor. The convection Mach number is defined as the ratio of the convection velocity to the speed of sound of the ambient medium and is the convection Mach number of the large eddies in the jet.

Researchers such as Ribner [25], Goldstein and Howe [26], and Ffowcs-Williams and Maidanik [27] continued to make improvements on the acoustic analogy. The results of these improvements are summarized in more detail by Bailly et al. [28]. Further development of the acoustic analogy by Papamoschou et al. [10] have shown that the noise radiation efficiency is dependent on the turbulence intensity in the jet, the coherence of the structures in the jet, and the convection Mach number of the large structures. The noise radiation efficiency scales linearly with turbulence intensity while non-linearly with the convection Mach number. Papamoschou shows that for a 50% reduction in turbulence intensity, only a 3 dB reduction in noise is observed, while a 33% reduction in convection Mach number results in a 10-15 dB reduction in noise observed. Therefore, a reduction in convection Mach number would generate the largest reduction in radiated noise.

2.2.2. Radiating and Non-Radiating components

In order for fluctuations produced within the jet to radiate to the acoustic far field the disturbance causing the fluctuation, also called eddies, must be traveling faster than the speed of sound in the ambient medium [18]. Therefore not all fluctuations will radiate to the far field and generate noise. As the noise in the far field is of primary interest, a method for separating the radiating and non-radiating components is necessary. Transforming Lighthill's equations in the frequency-wavenumber space, as shown by Crighton [12], provides a method for determining the radiating components. In the frequency-wavenumber space all frequencies contained within the flow will radiate to the far field while only a portion of the wavenumbers will contribute to the far field noise. For each frequency the wavenumber that divides the radiating and non-radiating components can be found using Equation (2.9).

$$k_a = \omega / a_\infty \tag{2.9}$$

Since the disturbance must be traveling faster than the ambient speed of sound the wavenumbers that radiate will be less than the wavenumber corresponding to the ambient speed of sound for a given frequency found using Equation (2.9), which provides a method for filtering the radiating and non-radiating components of the near field pressure. This approach was used by Tinney and Jordan [17] on near-field acoustic microphone measurements. Tinney and Jordan identified two characteristics of the radiating components being a low-frequency, coherent component that radiates at large angles to the jet axis and a high-frequency, less coherent component that radiates at small angles to the jet axis.

More recently Du and Morris [29] developed a method to separate radiating and non-radiating components from simulation data. Characteristics of the radiating and non-radiating field are found through comparison of noise sources inferred from the far field to noise sources inferred from the near field. Using a wavepacket model to represent the noise sources for both methods, pressure field results from the wavepacket model inserted into the wave equation found good agreement with CFD results. A main difference in the noise sources found were the convection speeds. The near field results had lower convection speeds due to the non-radiating components.

2.2.3. Large Scale Structures in Turbulent Jets

Flow visualization experiments conducted by researchers such as Mollo-Christensen [30], Brown and Roshko [15], and Papamoschou and Roshko [31] revealed the existence of large turbulent structures in shear layers of jets. Multiple researchers noted that from flow visualization the structures typically had one convection speed in its lifetime. Additional experimental studies by McLaughlin et al. [32] showed that the structures observed were non-deterministic in both space and time and appeared as trains of vortices with initially increasing amplitude upon exiting the nozzle then eventually decaying as the vortex moves downstream.

Studies by Tam and Morris [33] showed that these large structures can be modeled as instability waves. Using the instability waves as a model, Tam and Morris were able to create a solution that coupled the near and far field and showed that the large scale structures are important for noise generation. Tam et al. [34] have shown that the far field spectra from microphone measurements of jets can be decomposed into two similarity spectra: one for small scale turbulence termed the fine scale spectra (FSS), and one for large scale structures termed the large scale spectra (LSS). At large polar angles to the jet axis a combination of the FSS and LSS fits spectra well, while at small polar angles to the jet axis, the dominant noise direction, the LSS fits the spectra well which has a peak at low frequencies. From these measurements it is clear that large scale structures are important for noise generation in the dominant noise direction. Applying the similarity spectra to microphone measurements Morris [35] was able to generate wavenumber spectra using an acoustic analytical model which demonstrated the effect of radiating and non-radiating components in jet noise.

Crighton and Huerre [36] demonstrated that a windowed, sinusoidal wave serves as a basic model for the large scale structures observed in jets. This wavepacket model will produce noise in the far field for both supersonic and high subsonic conditions, and also predicts the directivity of the noise radiation. The importance of the windowing is shown through supposing a wavepacket with no windowing with a single frequency. The wavenumber spectrum will be a discrete value, shown in Figure 2.2.

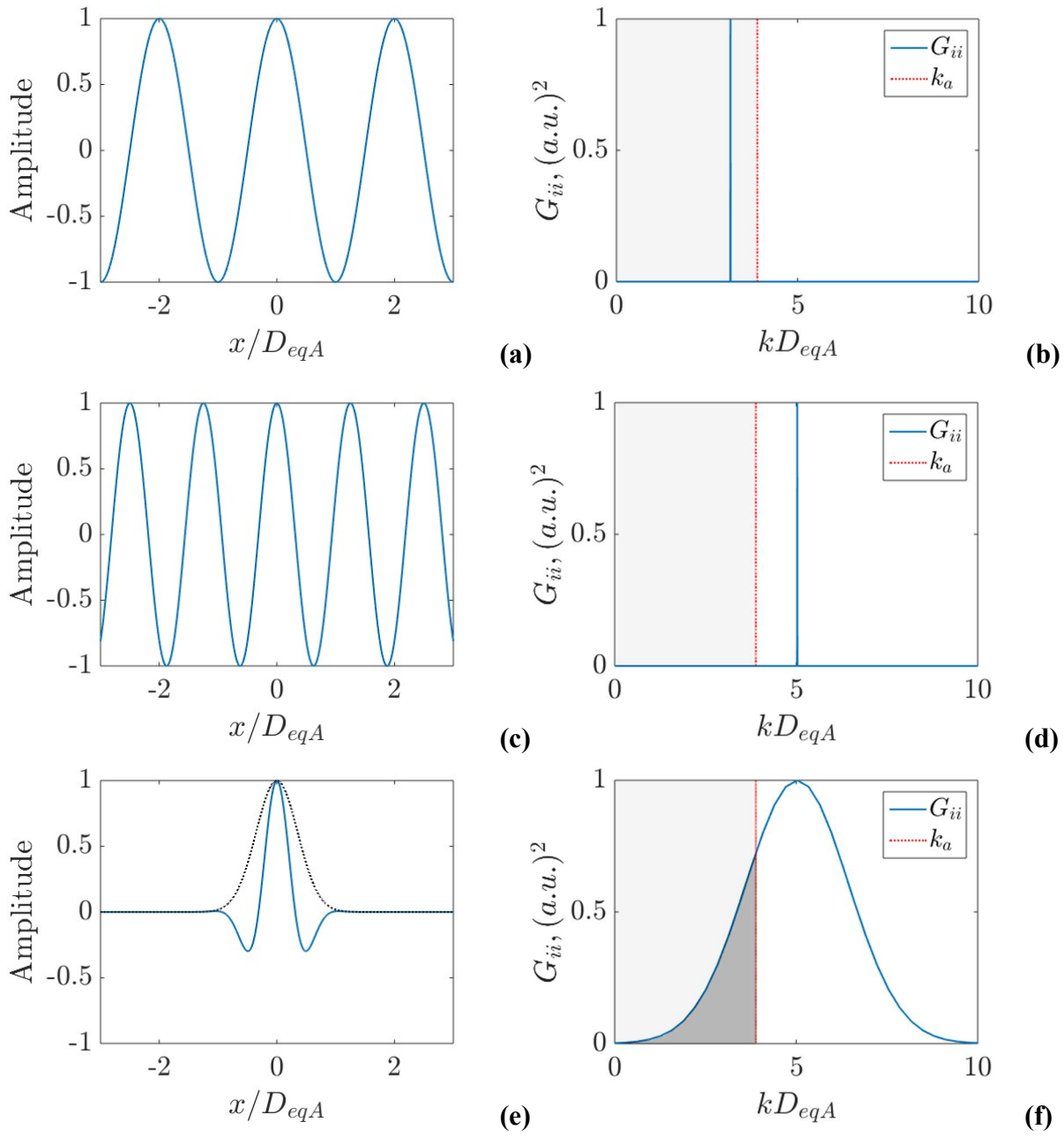

Figure 2.2. Diagram of noise generation for wavepackets (a) sinusoidal wave with supersonic convection speed (b) wavenumber spectrum for wave with supersonic convection speed (c) sinusoidal wave with subsonic convection speed (d) wavenumber spectrum for wave with subsonic convection speed (e) Gaussian windowed sinusoidal wave with subsonic convection speed (f) wavenumber spectrum for Gaussian windowed sinusoidal wave. The red line denotes the division between radiating and non-radiating components, wavenumbers below the line radiate, the shaded region, will radiate

For wavepackets traveling with a supersonic convection speed, it will radiate to the far field since the wavenumber of the single frequency wavepacket is less than the wavenumber based on the speed of sound. This is shown in Figure 2.2b, where the red vertical line denotes the wavenumber that divides the radiating and non-radiating components. Wavenumbers below the line, in the shaded region, will radiate. If the wave were traveling with a subsonic convection speed then the wavepacket will not radiate to the far field, shown in Figure 2.2d. Applying a windowing function such as a Gaussian window to the sinusoidal wave results in the wavenumber spectra to no longer be discrete. The windowing causes the wavepacket to have a range of wavenumbers, shown in Figure 2.2f. The range of wavenumbers causes a broadband spectrum, so even wavepackets with subsonic convection speeds may radiate a portion of their energy to the far field [37].

This method of noise generation is especially important for heated, high-subsonic jets. In heated jets the speed of sound in the jet is increased due to the temperature so that even if the Mach number of the jet is subsonic, the large structures in the jet are still traveling faster than the ambient speed of sound [20]. This fact is important especially for the current work as the jet has a high subsonic Mach number but the jet is heated to three times the ambient temperature. Additional research has found that although large scale structures, which wavepackets model, contain less of the overall turbulent energy in jets, these coherent structures are more acoustically efficient than disorganized structures [18].

Researchers have used wavepackets in acoustic models to represent structures observed in jets. A detailed look into evidence of wavepackets and applications of wavepackets by other researchers is given by Jordan and Colonius [18]. Du and Morris [29] used a wavepacket model as the boundary conditions to the 3D pressure wave equation and successfully obtained pressure levels in the far field that were in good agreement with pressures predicted by numerical CFD solvers. Kastner and Samimy [38] used a modified wavepacket model to model the noise events from microphone measurements that were found to correlate with the breakdown of structures observed using a MHz rate imaging system. The modified wavepacket model successfully reproduced the trend seen in the correlations between the MHz imaging system and the microphone measurements.

2.3. Multi-Stream Jets

Most jets from aircraft engines contain more than one stream. Most current aircraft engines contain both a core stream and a bypass stream. The additional stream changes the jet plume and causes noise reductions. The additional momentum from the bypass stream causes turbulent mixing with the core and slows down the convection speeds in the flow. For heated, high speed jets the slowing of convection speeds can cause the structures to become subsonic with respect to the ambient medium [39]. Therefore, noise reductions due to secondary streams are considered to be due to slowing of convection speeds in the shear layer. As explained in Section 2.2.2 when the convection velocity is subsonic the noise will not radiate to the far field.

While current aircraft engines only contain up to two streams, future engines for supersonic transport vehicles may contain a third stream [2]. Studies by Henderson [3] have shown that three stream nozzles reduce high frequency in both the peak noise direction and at side angles to the jet. Additional studies by Henderson et al. [5] showed that the tertiary stream had the largest noise reduction when the area ratio of the bypass to the core was low. Additionally, the noise reduction was greatest when the core was at supersonic conditions and when a forward flight Mach number was not simulated.

For both secondary and tertiary streams numerous researchers have shown that offsetting the secondary or tertiary stream to create a locally "thicker" stream on one side and a locally "thinner" stream on the opposite side offer additional noise reduction potential. Computational studies by Dippold et al. [7] demonstrated that the thicker side of the jet had reduced turbulent kinetic energy. Papamoschou et al. [4] developed models for three stream jets with offsets which highlighted the importance of proper determination of convection Mach number. Henderson et al. [5] conducted acoustic measurements on three-stream jets and three-stream jets with an offset. The measurements showed up to an 8 dB noise reduction was possible, comparing the tertiary offset configuration with an axisymmetric two stream configuration. Henderson and Wernet [40] characterized the flow using PIV measurements and showed a reduction in turbulence intensity on the locally "thicker" side of the jet stream. Papamoschou and et al. [4] also studied three-stream jets with offsets. Acoustic measurements showed that axisymmetric three-stream jets did not offer any benefit for noise reduction, while offset configurations offered up to 5.1 dB reduction.

Recent studies by Papamoschou and Phong [41] of the convection velocity in offset two stream jets showed that adding the secondary stream reduced the convection velocity greatly in the first few nozzle diameters. It was concluded that the reduction in convection velocity resulted in the primary potential core no longer being a dominant noise source; rather the secondary shear layer became the dominant noise source. Additionally, when the secondary stream was offset, an elongation of the secondary potential core is observed while the primary potential core is reduced. The reduction of the convection velocity was determined as the mechanism causing the noise reduction observed in offset configurations.

3. Review of Correlation Measurements in Jets

Correlation measurements have been used extensively in the study of jet noise for the purposes of noise source identification and convection velocity calculation. Correlations between noise events with flow events have been used as a means to identify noise sources within the flow. Noise events are measured using microphones while flow events are acquired from velocity or flow visualization measurements in the jet. A review of correlations used for noise source identification will be explained in Section 3.1. Two point space-time correlation measurements are used to calculate the convection velocity of turbulent structures in the jet. As explained in Section 2.2.1 proper determination of convection velocity is important for accurate acoustic predictions of jet noise. Section 3.2 gives a review of various techniques used to measure two point, space-time correlations for convection velocity determination. The process of calculating convection velocity using two point space-time correlations is described in Chapter 4.

3.1. Correlation Measurements for Noise Source Identification

Correlating events in the flow with microphone measurements in the far field is a method used to identify important noise producing regions of jets. Panda et al. [42] correlated various velocity and density signals in the flow with microphone measurements in the far field. The highest correlation between flow measurements and microphone measurements was when ρuu (a component of the Lighthill stress tensor) was correlated with the microphone measurements. The locations of strongest correlations were along the centerline. Correlations along the lip line (r/D = 0.5) were found to only be significant if the convection velocity of the turbulent eddies was

supersonic. A study by Hileman et al. [43] on an unheated, Mach 1.28 ideally expanded jet also identified the centerline as an important noise generation region. Using correlations between flow visualization images and microphone measurements, structures were identified just before a noise emission event. The structures were upstream of the end of the potential core and were observed to break down just prior to a noise emission event. Additionally, an increase in image intensity was observed just past the end of the potential core during the noise emission event. Hileman et al. suggest the breakdown of flow structures is caused by the interaction of the shear layers reaching the potential core which then cause noise emission.

Veltin et al. [44] correlated microphone measurements in the far field with flow visualization using Optical Deflectometry (OD) on a Mach 1.75 jet. Axial locations 4 diameters downstream and 10 diameters downstream of the nozzle exit were peak correlation locations. These locations correspond to points before and after the end of the potential core. Papamoschou et al. [45] also correlated OD flow visualization measurements with microphone measurements. Based on the correlations the shear layer was identified as a noise source region. It was also noted due to the directivity of the coherence that the convection speed of the turbulent eddies is an important factor in noise generation.

3.2. Correlation Measurements for Convection Velocity

Numerous researchers have measured convection velocity using space-time correlations of velocity signals or flow visualization measurements. Velocity measurements come from a variety of measurement techniques such as hot wire anemometry and advanced laser diagnostics. Flow Visualization methods include OD, Double-exposure planar-laser induced fluorescence (PLIF), and visualization from condensation of seed particles.

Davies et al. [46] measured two point, space-time correlations using hot wire anemometry on cold, subsonic jets. A radial profile for convection velocity was measured that differed from the mean velocity profile. In the core the convection velocity was lower than the mean, while at larger radial locations in the shear layer the convection velocity was greater than the mean velocity. Based on these results, the researchers concluded the assumption of Taylor's hypothesis (that the mean velocity and convection velocity are the same) used in many analyses does not hold for jets. Physically, a convection velocity lower than the mean in the core seems unlikely as pointed out by Lau et al. [47]. It is more likely that the hot wire probe, while in the core, was influenced by the

convection velocity of the slower moving structures in the shear layer. In this way the convection velocity measured in the core was lower than the mean. Overall, the convection velocity of the vortices in the shear layer was measured to be 60% of the isentropic exit velocity. Morris and Zaman [48] also used hot wire anemometry to calculate convection velocity in a cold, subsonic jet. Their measurements included a greater number of measurement locations and found a similar value for the convection velocity of turbulent structures of 62.3% of the isentropic exit velocity.

Although hot wire anemometry has been used successfully in high speed shear flows [49], taking measurements is still difficult due to the fragility of hot wires [50]. Additional difficulties arise in heated jets as the metals in hot wires can begin to oxidize in the high temperatures [51]. Due to these difficulties, advanced flow visualization and laser diagnostic techniques have been developed and used to measure convection velocity in high speed jets. Doty and McLaughlin [52] investigated convection velocity in unheated, high subsonic and supersonic jets using correlations from flow visualization from an OD instrument. Based on the flow visualization images two dimensional correlations showed the distinct large flow structures in the shear layer have convection velocities 75% of the isentropic exit velocity. Another study using OD measurements by Petitjean et al. [53] calculated convection velocities of structures in the shear layer to be between 72% to 74% of the isentropic exit velocity for unheated jets with a Mach number of 0.9. Kerhervé et al. [54] used LDV to measure convection velocity in unheated, supersonic jets. Radial profiles similar to those of Davies et al. [46] which showed convection velocities just below the mean velocity near the core while higher than the mean velocity in the shear layer were determined.

Measurement techniques such as Laser Velocimetry (LV), Time Resolved Particle Image Velocimetry (TR-PIV), TR-DGV, and Planar Doppler Velocimetry (PDV) have been used to measure convection velocities in heated jets. Lau [55] used LV and found heated jets had lower convection velocities, between 55% to 65% of the isentropic exit velocity depending on the axial location. He noted that for all jets the convection velocity increases axially until the end of the potential core where the convection velocity then decreases. Murakami and Papamoschou [56] used double-exposure planar-laser induced fluorescence (PLIF) system to measure convection velocity in supersonic jets with co-flow. The results, however, are not for true heated jets as the "heating" was simulated using an air/helium mixture. Adding a secondary stream resulted in a reduction in convection velocity from 70% to 62% of the isentropic exit velocity.

Bridges [57] used TR-PIV with a 25 kHz sampling frequency to study the effect of heat on space/time correlations in single stream jets. He noted the greatest impact of heat was on the potential core length; and therefore, once the change in potential core length for heated jet was accounted for, the majority of one point and two point correlations collapsed. Ecker et al. [58] measured convection velocity using TR-DGV in a heated supersonic jet. Radial profiles showed the convection velocity in the core very close to the mean velocity, while convection speeds in the shear layer were greater than the mean velocity. These radial profiles show the expected trend of eddies traveling at speeds close to the mean velocity in the core. This is expected because in the core the turbulence intensity is low and therefore small structures would travel at speeds very near the mean. Ecker et al. [59] developed a scaling method that successfully collapsed convection velocity results for heated and unheated conditions from various researchers such as Kerhervé et al. [54] and Morris and Zaman [48], and Ecker et al. [58].

The importance of proper seeding in convection velocity measurements was studied by Thurow et al. [60]. It was found in their studies that the seeding conditions can have a significant impact on the measured convection velocity. Comparing results of convection velocity from both correlation of PDV velocity signals and correlation of flow visualization images, which used natural condensation of seed particles to highlight flow features, resulted in different values depending on which parts of the jet were seeded. Results showed the importance of seeding the entire jet, including the co-flow. Using PDV and seeding all areas of the jet including the core, shear layer, and co-flow produced the most accurate results for convection velocity.

At the present, time resolved convection velocity results on high subsonic, heated multi-stream jets are insufficient. To the author's knowledge convection velocity has not been studied on these types of jets. Additionally, the convection velocity studies from previous literature have been at limited axial and radial locations. The current study provides convection velocities at a greater number of axial and radial locations for a more detailed mapping of the convection velocity distribution within the jet.

4. Methods

The following section describes the experiment set-up at AAPL along with the data processing and statistical approach for calculating the convection velocity. A wavepacket model is also introduced which will be used to provide insight into how the convection velocity of structures in the jet affect radiated noise.

4.1. Experimental Methods

Two component PIV was used to measure axial and radial velocity. For more details on the PIV setup and instrumentation see Henderson and Wernet [40]. Convection velocities were measured using the TR-DGV instrument developed by Ecker et al. [61] The system uses 2 laser planes and 2 photomultiplier (PMT) array detectors. The system uses a tunable, continuous wave Verdi V18 laser as the light source. Two overlapping laser sheets create the planar measurement region. The light sheets are multiplexed with a time difference of 2 μs, and flow was sampled for 1 s with a sampling rate of 250 kHz. The multiplexing of the laser sheets was accomplished using two IntraAction Corp. 80 MHz acousto-optical modulators (AOMs).

The multichannel PMT cameras consist of a two Hamamatsu H8500C PMT array detectors with 64 channels on each detector. For this experiment only 32 channels were used on each detector with 4 channels in the axial direction and 8 channels in the radial direction. The PMT detectors were oriented perpendicular to the measurement plane, with one on each side of the measurement plane. As shown in Figure 4.1, the light entering the PMT camera is split with one path entering an iodine cell before reaching the PMT array detector. The other path is redirected with a mirror and goes directly to the second PMT array detector. The focal length of the camera lens used in this experiment was 200 mm resulting in a magnification of approximately 1.4. This imaging configuration allowed for a measurement plane 34.88 mm (1.37”) in the axial direction and 69.76 mm (2.75”) in the radial direction.

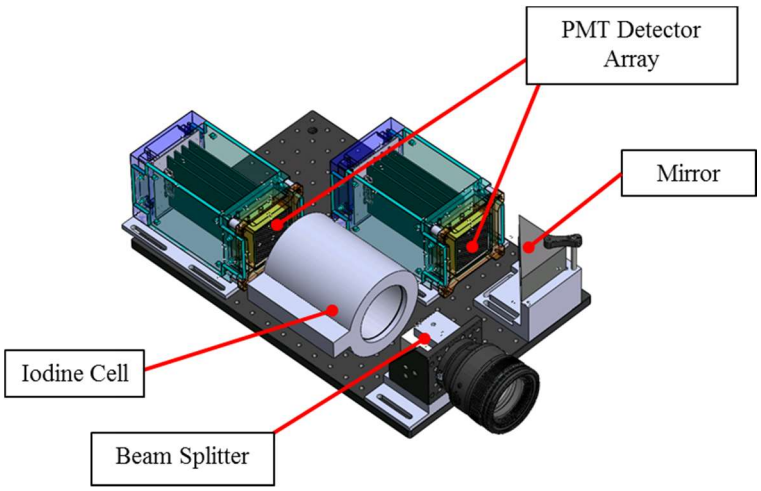

Figure 4.1. PMT Camera assembly

The experiment was conducted at AAPL at NASA Glenn Research Center. The three-stream nozzle configurations were installed on the High Flow Jet Exit Rig (HFJER) in the Nozzle Acoustic Test Rig (NATR). The nozzles used are externally-mixed and externally-plugged as shown in Figure 4.2. The red area denotes the heated, core flow. The blue areas denote the unheated bypass and tertiary flows. The area ratios and characteristic diameters of the nozzles are given in Table 4.1. The subscripts, c, b, and t are used to denote the core, bypass, and tertiary streams, respectively. These dimensions are the same for both the axisymmetric and asymmetric configuration. To create the asymmetry nozzle configuration, the tertiary stream was offset by 0.156" to create a locally "thick" side [11]. Figure 4.3 enlarges the tertiary stream to better see the radial offset of the tertiary stream. Typically the diameter of the nozzle is used to present results in non-dimensional units; however, since the nozzles studied are externally-plugged, an equivalent diameter is calculated based on the nozzle area. The equivalent diameter, D_{eqC}, is based on the area of the core while the equivalent diameter, D_{eqA}, is based on the total area of the three stream nozzle.

Table 4.1. Nozzle Geometry

D_{eqC} (in)	D_{eqA}(in)	A_b/A_c	A_t/A_c
5.2	7.87	2.5	1.0

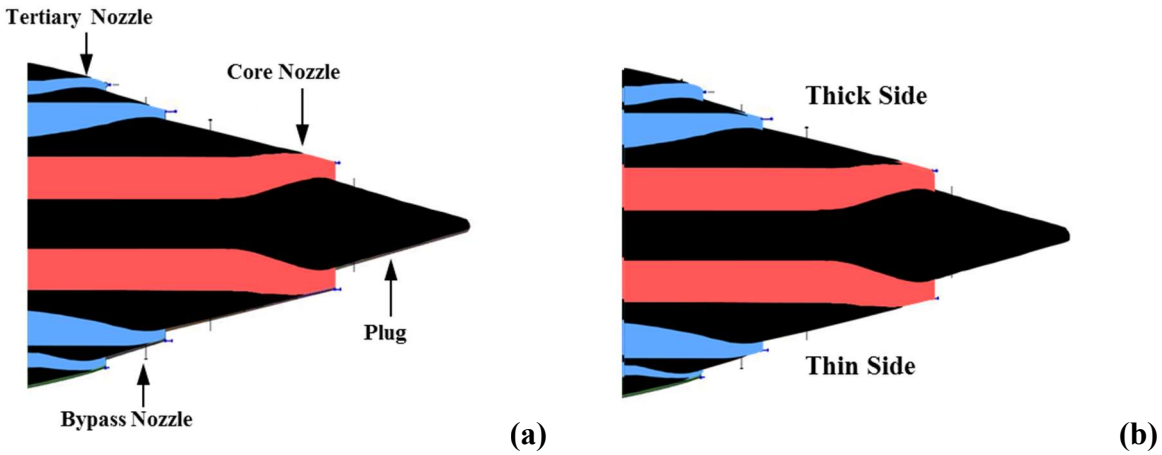

Figure 4.2. Three-stream nozzle configurations (a) axisymmetric (b) asymmetric with tertiary offset

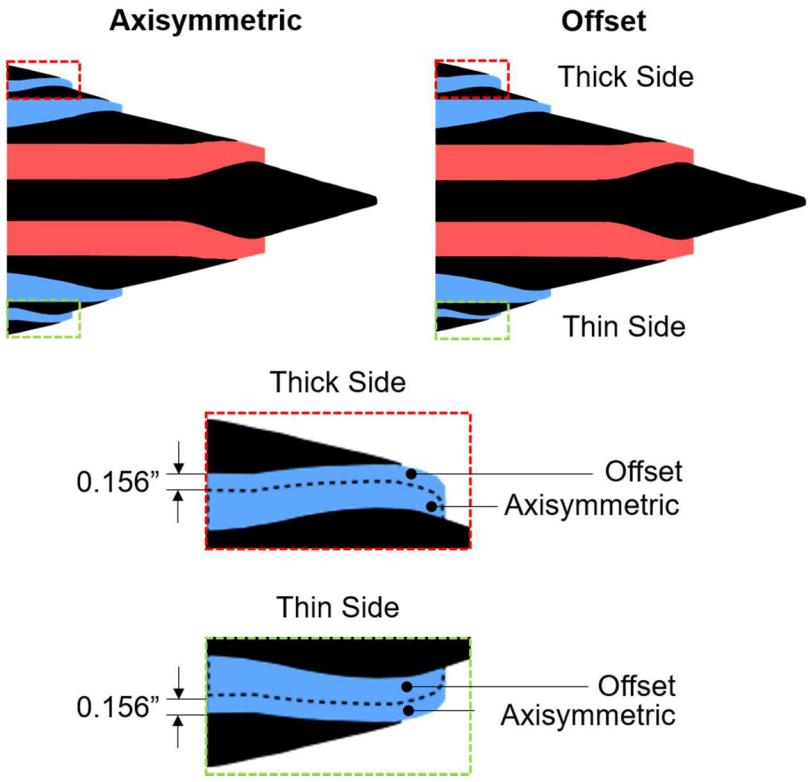

Figure 4.3. Three-stream nozzle configurations with enlarged tertiary streams. The red box denotes the thick side of the offset configuration and the green box denotes the thin side of the offset configuration

The flow was seeded using three different systems: one for the core, one for the bypass, and one for the tertiary stream. The core and bypass were seeded with alumina powder, and the tertiary

stream was seeded with a pH stabilized aluminum oxide dispersion [62]. When the laser light hits the particles the light is scattered and collected with the multichannel PMT cameras.

Table 4.2 lists the operating conditions of the jet for the configurations tested. The nozzle pressure ratio (NPR) is defined as the total pressure divided by the ambient pressure. The nozzle temperature ratio (NTR) is the total temperature divided by the ambient temperature. For the axisymmetric nozzle configuration PIV data was provided by Henderson and Wernet to allow for convection velocity results from the Virginia Tech TR-DGV instrument to be compared to PIV mean velocity and turbulence intensity results collected by NASA [40].

Table 4.2. Operating Conditions

	NPR_c	NPR_b	NPR_t	NTR_c	NTR_b	NTR_t	Measurement Type
Axisymmetric	1.8	1.8	1.4	3.0	1.25	1.25	TR-DGV/PIV
Offset	1.8	1.8	1.4	3.0	1.25	1.25	TR-DGV

Table 4.3 lists the jet conditions. The conditions are the same for both the axisymmetric and the offset nozzle configurations.

Table 4.3. Jet Conditions

U_j (m/s)	a (m/s)	a_∞ (m/s)	M_j	Re
519	542	335	0.956	1.42×10^6

The TR-DGV instrument was mounted to a traverse to sample the flow at many axial locations to measure the majority of the jet plume. For all tested conditions, the instrument was moved to 4 distinct radial locations. A model of the TR-DGV system installed at AAPL is shown in Figure 4.4.

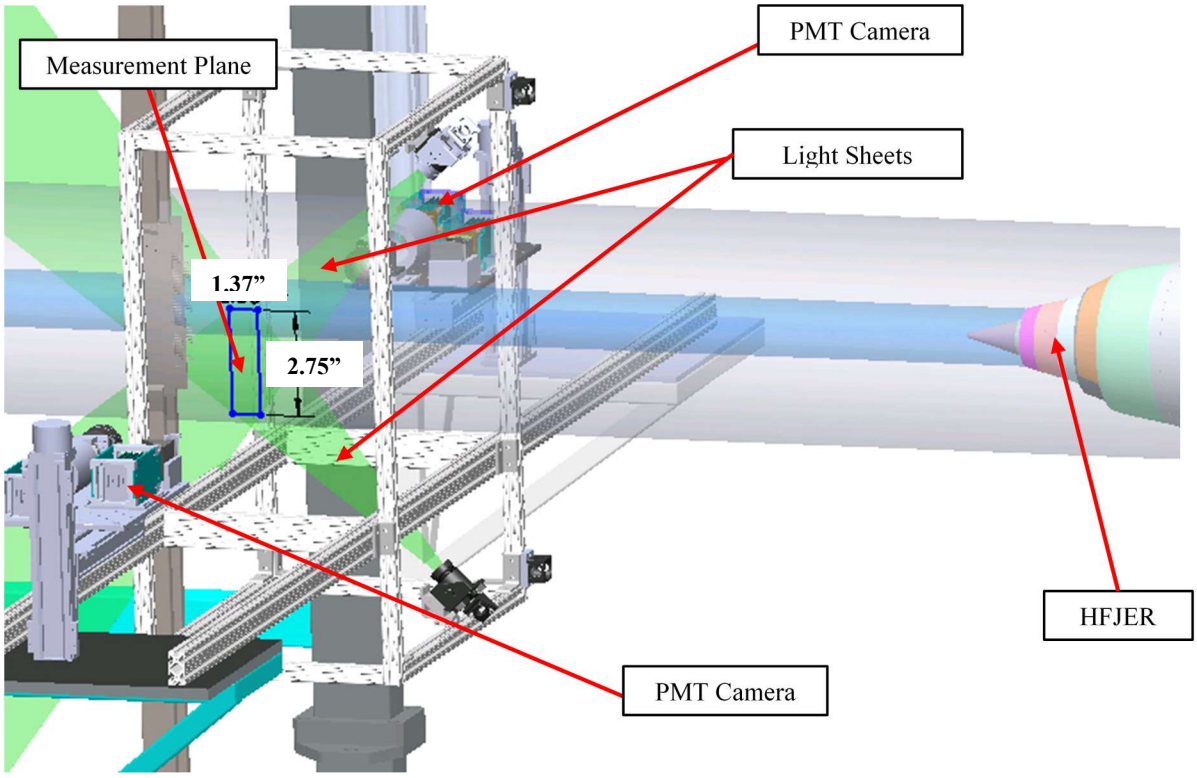

Figure 4.4. TR-DGV Instrument Installed at AAPL in the NATR

4.2. Statistical Methods

A new method was used to calculated convection velocity. This new method used the seeding signal instead of the traditional method which uses the Doppler-shifted velocity signal. The seeding signal is extracted from the raw signal recorded by the PMT detector without the iodine cell. The seeding signal contains information about the turbulent structures because the bursts of seed particles are convected with the turbulence in the jet flow. Due to the multiplexing of the laser sheets, the raw signal contains data when both lasers were on and off. An example of a pair of laser pulses from the raw signal is shown in Figure 4.5. For each raw signal from the unfiltered PMT detector, two seeding signals can be obtained, one for each laser. The seeding signal for each laser was extracted from the PMT detector raw signal by taking the mean value when the laser was on and subtracting from it the mean value when the laser was off. This was done for each laser pulse to obtain a seeding signal for each laser with a record length of 200,000 samples.

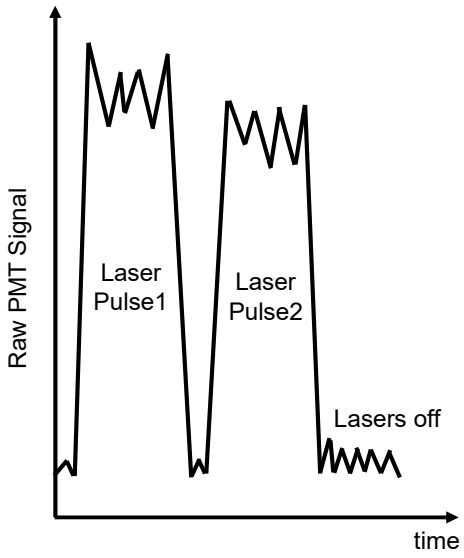

Figure 4.5. Example of raw signal from unfiltered PMT detector

Through the use of the TR-DGV system the seeding signal was obtained for each of the 32 pixels simultaneously at each axial location. A second order space time correlation function can be calculated using the following definition [48]:

$$R_{ij} = \frac{1}{T}\int_{-T/2}^{T/2} s_i(x,r,t)s_j(x+\varsigma, r+\xi, t+\tau)dt = \overline{s_\iota(x,r,t)s_j(x+\varsigma, r+\xi, t+\tau)} \quad (4.1)$$

Where T is the data acquisition time period, s is a generic mean flow fluctuation variable (in this case the fluctuation of the seeding signal), ς is the correlation streamwise spacing, ξ is the correlation radial spacing, τ is the correlation lag time, and the bar denotes time averaging.

The convection velocity of the eddies can be calculated using a second order space/time correlation function as shown by Ecker et al. [58] The correlation is calculated at each x/D location, for each $\Delta x/D$ spacing provided by the four streamwise pixels at a given r/D location in the flow. Therefore, for each x/D location, the space/time correlations across the sensor in the axial direction can all be plotted on one figure with τ as the independent variable.

Since the correlation functions have maxima along the convection ridge, the equation $\varsigma_r = U_c\tau_r$ can be used to solve for the convection velocity, U_c. The spacing between pixels, Δx, is known, so the equation can be rewritten as $U_c = N\Delta x/\tau_r$. The slope, $\Delta x/\tau_r$, can be determined from the aforementioned plots of the correlation functions [63]. Extracting the maxima of the correlation curves using a cubic spline and plotting the correlation lag time on the x-axis versus

spacing on the y-axis allows a linear least squares fit to be performed on the four points. The resulting slope of this line is the measured convection velocity. This process is shown in Figure 4.6. The uncertainty in the calculation of the convection velocity is ±0.07 $\delta U_c/U_c$. Details on the uncertainty analysis are given in the Appendix.

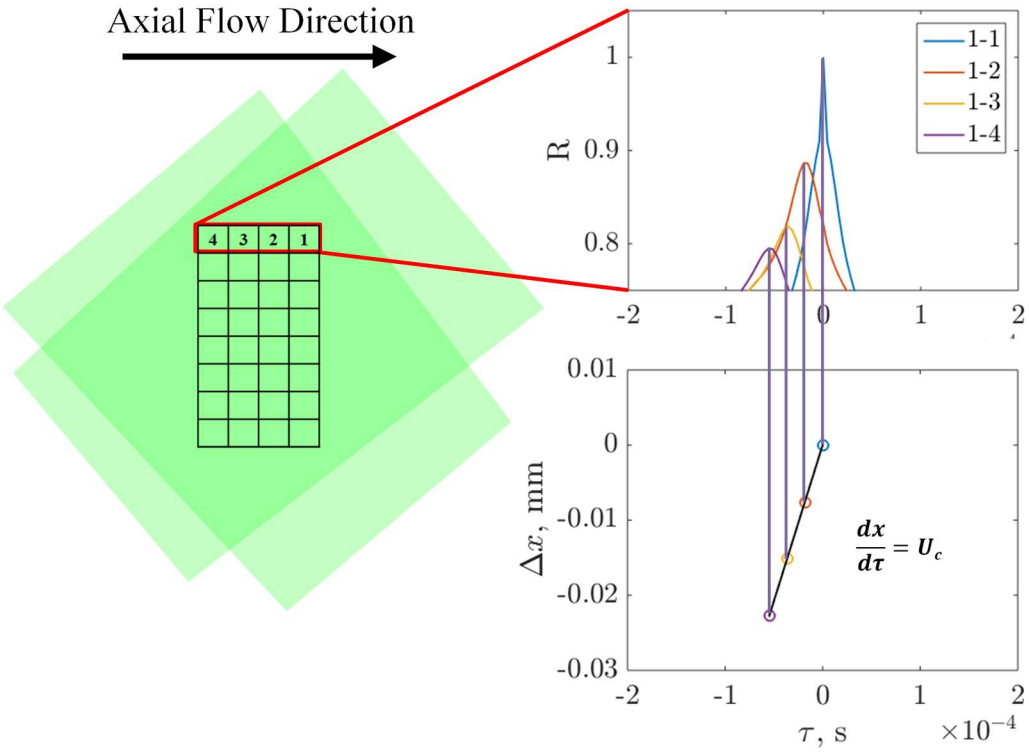

Figure 4.6. Schematic of processing for calculating convection velocity

The above explained method of calculating the convection velocity from the space/time cross-correlation of the seeding signal is different than the common velocity measurement technique PIV which measures the true velocity of the flow. Although both the proposed method for calculating the convection velocity and PIV use space/time correlations of seed based signals, they provide measurements of different velocities of the flow. In PIV the time delay over which space/time correlations are measured is small compared to the time scales of interest in the flow. Because of the small time delay, Taylor's hypothesis is valid which means that the convection velocity and the true velocity are equal. For the seeding signal from the TR-DGV instrument, the space/time correlations are over a much longer time so Taylor's hypothesis to no longer valid. Since the space/time cross correlations are over a larger time, the velocity calculated includes the effects of convection, allowing the convection velocity on the convective ridge to be calculated.

4.3. Wavepacket method

A wavepacket model is used to understand the effect convection speeds have on the radiated noise. Wavepackets are used to represent the pressure instability on the edge of the jet [64]; however, since near field pressure data is not available for this work, convection velocity from the seeding signal space/time correlations is instead used for this model. Past work by Picard and Delville [65] has shown that pressure and velocity instabilities are directly coupled. The wavepacket model used is based on the model proposed by Crighton and Huerre [36], and models the noise radiated in the peak noise direction. The wavepacket model used is a sinusoidal cosine function with a Gaussian window, given in Equation (4.2).

$$S(x) = \cos\left(\omega t - \frac{\omega(x - x_0)}{U_c}\right)\exp\left(-\frac{(x - x_0)^2}{l^2}\right) \tag{4.2}$$

This model uses a constant convection speed and characteristic length, given in Table 4.4. The characteristic length of the wavepacket was determined by making the approximated width of the wave packet one nozzle diameter. Another assumption of this model is the wavepacket width. The choice of wavepacket width will influence the results It is important to note that the width of the wavepacket chosen may bias the results, however, the width chosen for this study is similar to those used by past researchers [64]. The frequency is determined based on the range of Strouhal numbers typically seen in jets [35]. The convection velocities chosen for the study are based off chosen for the study are based off the convection speeds along the convective ridge in key areas that will be identified and explained in Section 5.3

Table 4.4. Model Parameters

l	St	U_c
$D_{eqA}/2$	0.05-1.0	$0.56U_j$ - $0.80U_j$

An example waveforms are given in Figure 4.7. From the wavepacket model a wavenumber spectrum can be determined. Using the method explained by Crighton [12] the components that are most likely to radiate are determined from the wavenumber spectrum as explained in Section 2.2.2. Although the wavenumber spectrum determined is not the true wavenumber spectrum of the pressure fluctuations, information about the radiating components can still be extracted because of the coupling between the kinetic energy and pressure energy. Based on the wavenumber spectra,

the speed of sound in the ambient medium, and Strouhal number, the percent of the wavenumber spectrum likely to radiate.

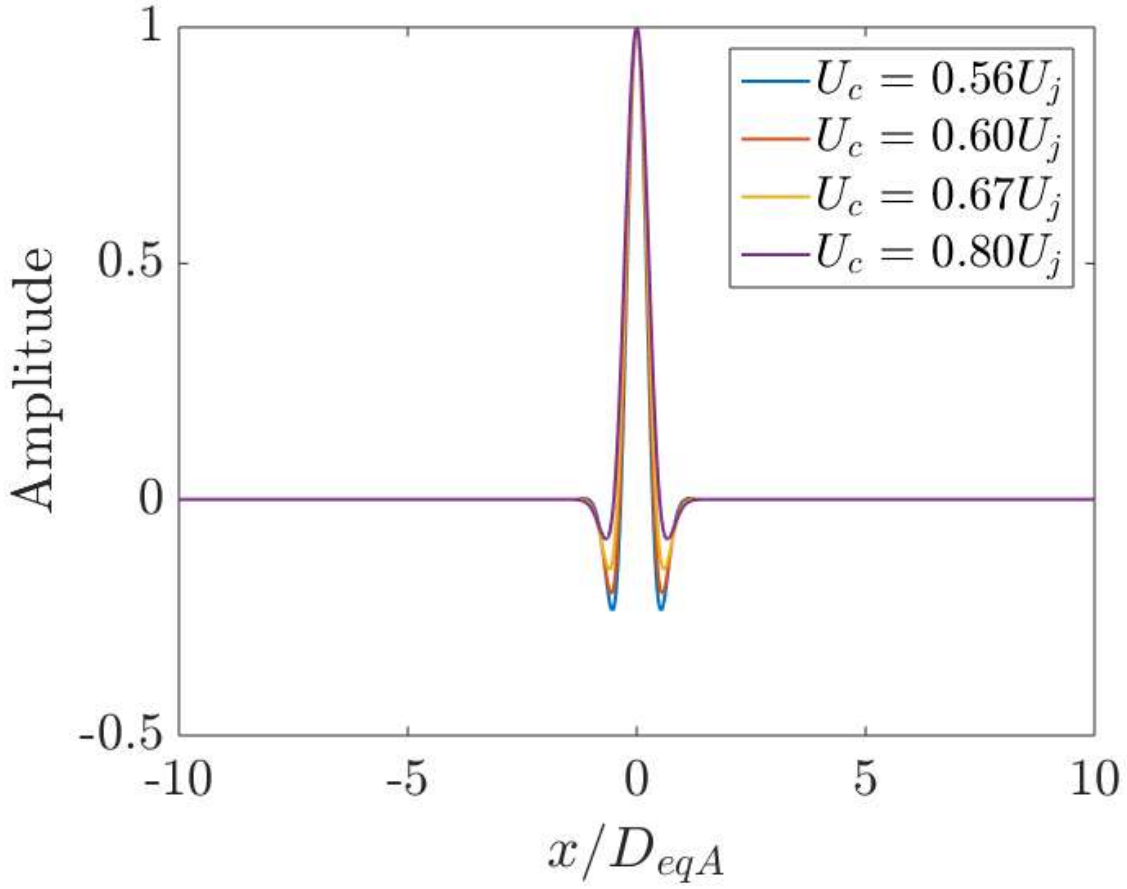

Figure 4.7. Wavepacket Form for St = 0.4 for various convection velocities studied

5. Results and Discussion

Results from the analysis methods described in the previous chapter are presented in the following sections. Section 5.1 contains results for solely the axisymmetric nozzle configuration. For the axisymmetric nozzle configuration NASA PIV results were available for comparison with Virginia Tech (VT) TR-DGV convection velocity results. Through the comparison of the NASA and VT data sets, areas are identified as key regions for noise sources. In Section 5.2 VT DGV

convection velocity results for the offset nozzle configuration are discussed and compared to the axisymmetric convection velocity results. Section 5.3 discusses the results from the wavepacket model. Fundamental mechanisms responsible for the noise generation in the axisymmetric nozzle are discussed along with explanations for the noise reductions observed due to the offset nozzle configuration. Acoustic measurements were made for the nozzle configurations that were studied for this thesis by Henderson et. al [5]. Although for the nozzle configurations and conditions studied in this thesis only had reductions on the order of 1 dB to 2 dB [5], the results to be presented in this section show that the measurement and analysis techniques are sensitive to small changes in noise levels. This is a promising finding since moving forward these measurement and analysis techniques are likely to identify the differences driving noise reductions in three stream axisymmetric and offset nozzles.

5.1. Axisymmetric Nozzle Configuration

For the axisymmetric configuration, the NASA PIV mean velocity and turbulence intensity distributions are shown in Figure 5.1 and Figure 5.2, respectively. Both the mean velocity and turbulence intensity data are nondimensionalized by the isentropic exit velocity. The axial and radial coordinates have been nondimensionalized by the equivalent diameter based on the total area of the nozzle, D_{eqA}. As the flow exits the nozzle the core and the bypass streams are visible in the NASA PIV mean velocity data. The flow exits the nozzle in the core very close to the isentropic exit velocity and maintains its velocity until about 5 diameters downstream.

The potential core regions of the core and secondary streams are clearly visible in Figure 5.2, as the potential core is characterized by the low turbulence intensity region. From the PIV data it is observed that the tertiary stream seems to mix with the secondary stream at an early axial location, as a distinct tertiary stream is not visible in either the turbulence intensity or the mean velocity distributions. Based on the turbulence intensity data, the potential core seems to begin to be overcome by the shear layers just after 5 diameters downstream, which is where the turbulence intensity along the centerline begins to increase.

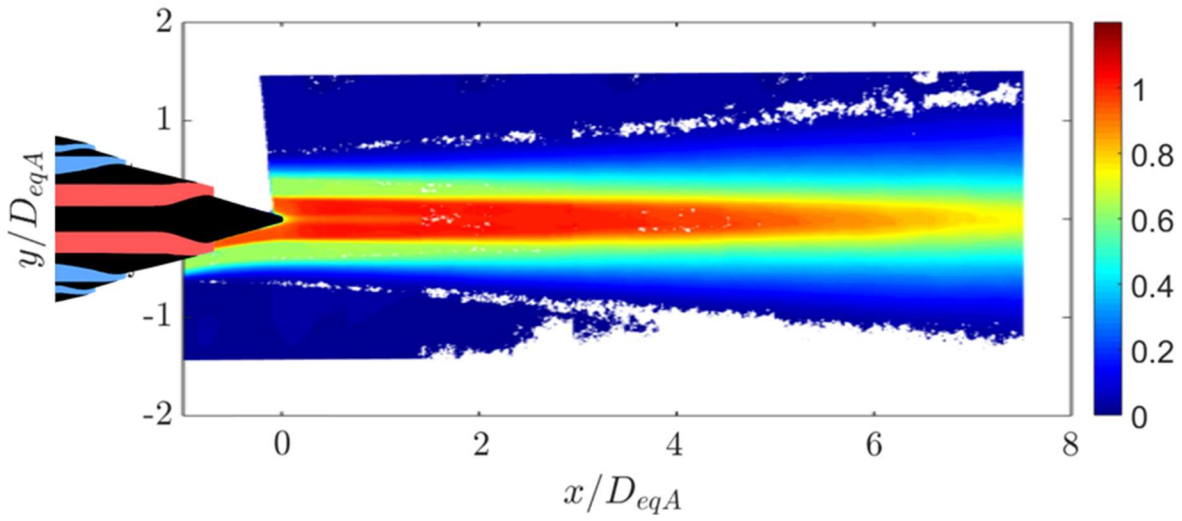

Figure 5.1. NASA PIV mean velocity, U/U_j, for the axisymmetric nozzle configuration

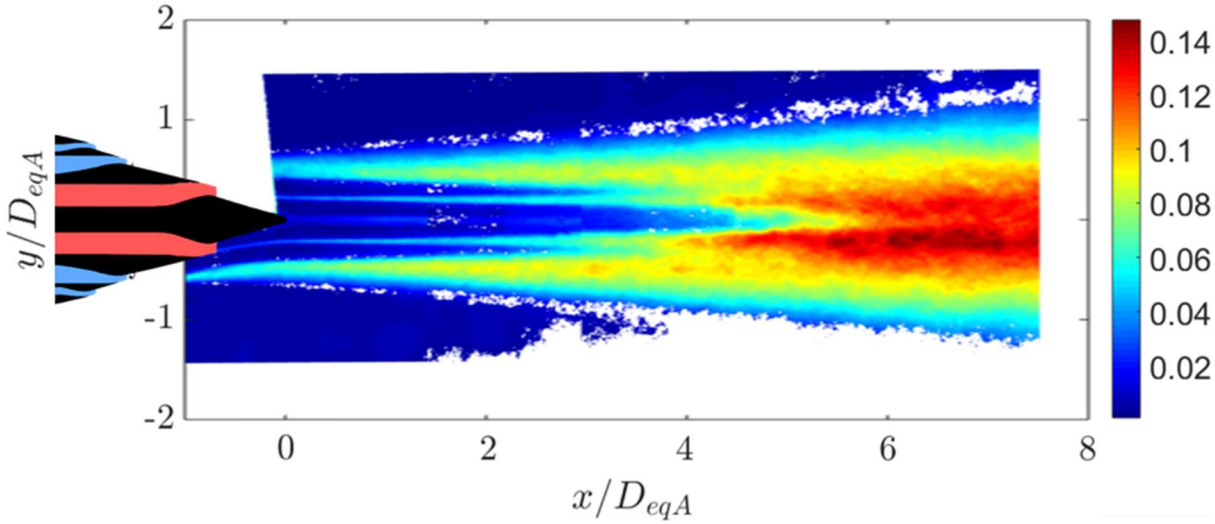

Figure 5.2 NASA PIV turbulence intensity, u'/U_j, for the axisymmetric nozzle configuration

The VT TR-DGV convection velocity data is compared to the NASA PIV mean velocity in Figure 5.3. The convection velocity data have been nondimensionalized by the isentropic exit velocity. Again, the axial and radial coordinates have been nondimensionalized by the equivalent diameter, D_{eqA}. A lag between the VT TR-DGV convection velocity and the NASA PIV mean velocity is observed in Figure 5.3. Even though the mean velocity decreases along the centerline of the jet, the convection speed of the turbulent structures persists for a longer distance. Although

more noticeable at larger axial locations, the convection velocity tends to be greater in the outer portion of the shear layer. This trend has been observed in previous studies [27,45,53], and is attributed to the entrainment of turbulent eddies with the shear layer which re-energize the shear layer.

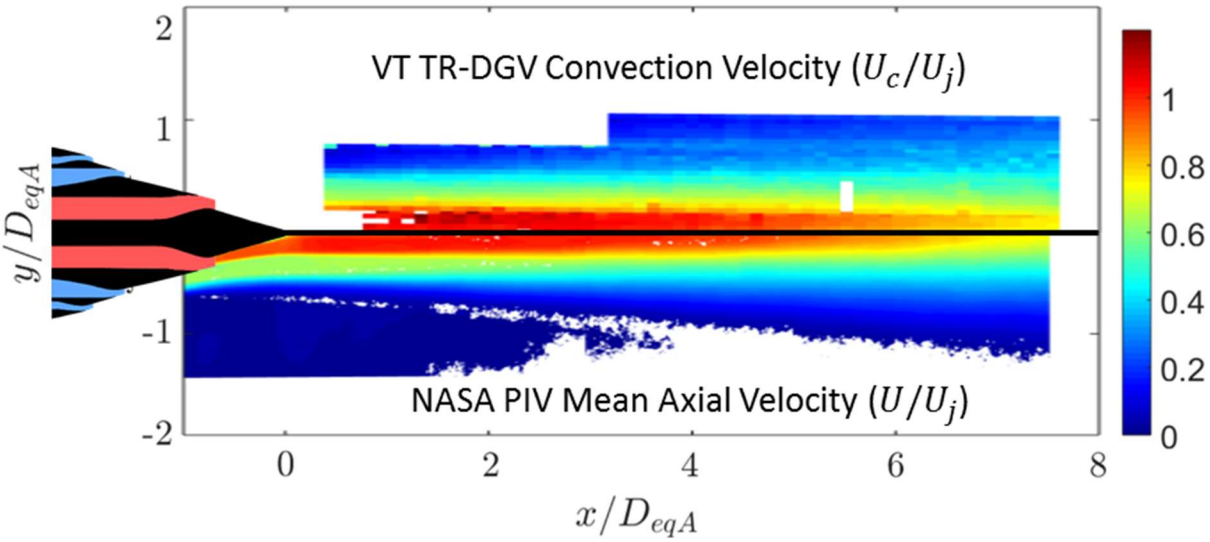

Figure 5.3 Comparison of VT TR-DGV convection velocity to NASA PIV mean velocity, for the axisymmetric nozzle configuration

Radial profiles of the NASA PIV Mean Velocity, NASA PIV turbulence intensity and VT TR-DGV convection velocity are shown in Figure 5.4. The radial profiles show the gradual increase in convection velocity over the mean velocity as the axial location is increased. Near the nozzle exit and close to the centerline, the convection velocity follows the mean velocity, which is expected since turbulence intensity is low in the potential core. These results are consistent with those reported by Ecker et al. [58] At greater radial locations, the convection velocity deviates from the mean. The deviation is due to a rise in turbulence intensity levels caused by the instabilities generated in the shear layer of the jet collapsing the potential core.

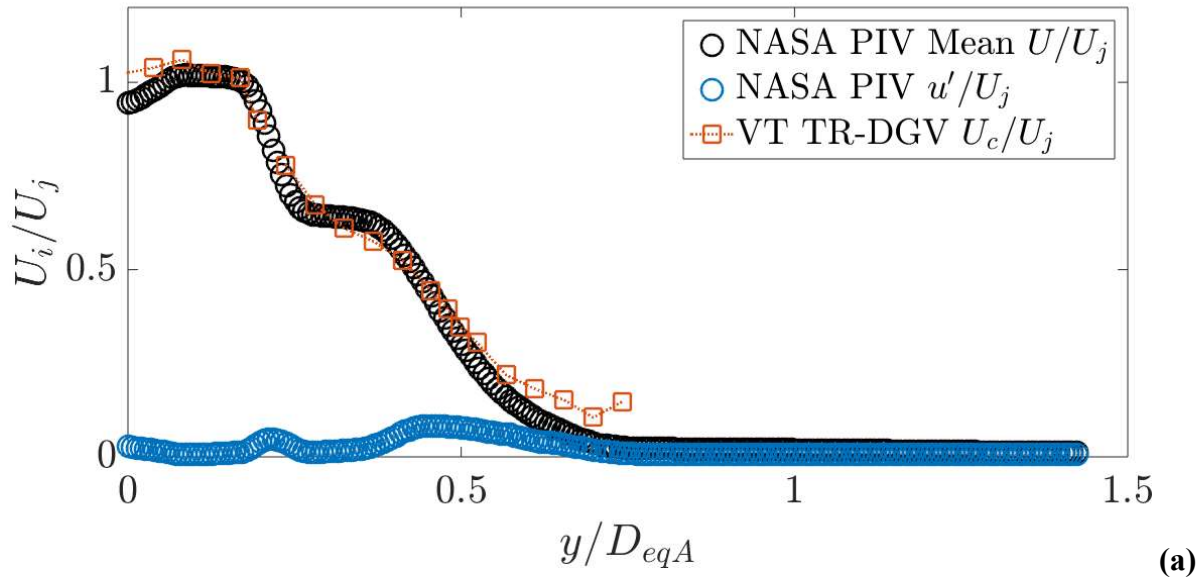

(a)

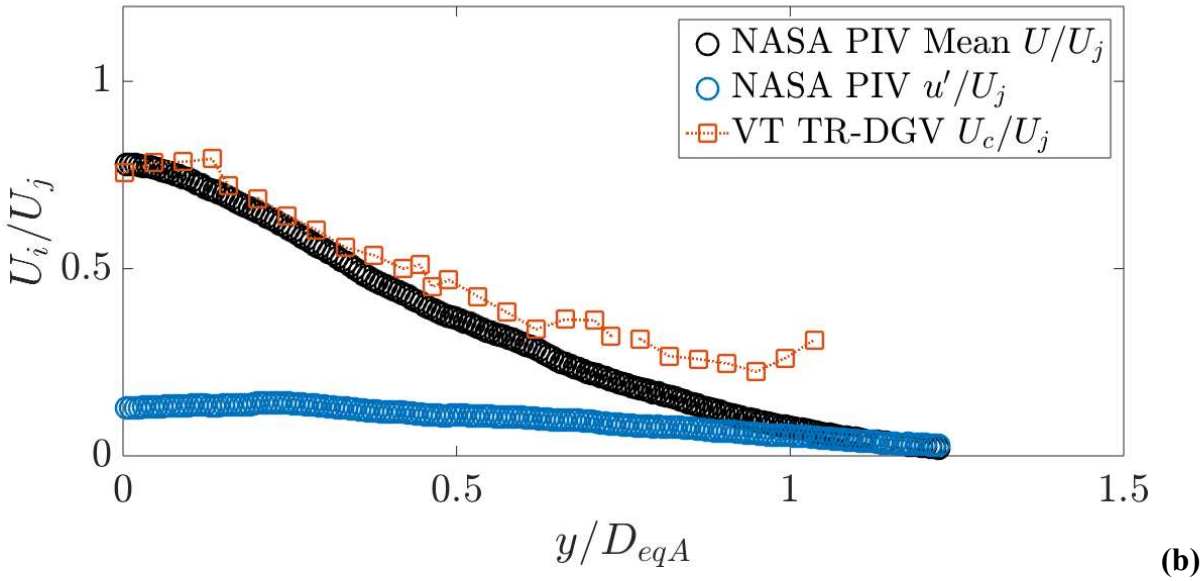

(b)

Figure 5.4. Radial contours at (a) x/D_{eqA}=1.0 and (b) x/D_{eqA}=7.0

As shown through Lighthill's acoustic analogy and associated stress tensor, areas of large velocity fluctuations are important for noise generation [22]. As discussed in Section 2.2, however, in order for disturbances in the flow to reach the far field, they must be traveling at supersonic convection speeds with respect to the ambient medium [18]. Therefore, not only are areas of high turbulence intensity of interest, but also areas of high convection speeds are of interest for noise generation in jet plumes. Further the radiation efficiency developed by Papamoschou et al. [10]

showed that both the turbulence intensity and convection velocity contribute the amount of radiated noise in jets. Therefore, comparison of the convection velocity distribution to the turbulence intensity distribution offers insight into regions of the jet most likely to be important to noise radiation.

To make this comparison, first the NASA PIV turbulence intensity distribution is converted from a filled contour to a line contour plot shown in Figure 5.5. The VT TR-DGV convection velocity data is reproduced in Figure 5.6. Note that the background of the figure where no data is available is colored gray. The line contours of the NASA PIV turbulence intensity data is overlaid on the VT TR-DGV data in Figure 5.7. From the overlaid contours, areas of both high convection velocity and high turbulence intensity are downstream of the end of the potential core, from x/D_{eqA} = 4 to 6 offset from the centerline around y/D_{eqA}= -0.1. These findings suggest this region along the centerline is an important location in the jet plume for noise production. Further, the identified region is consistent with correlation measurements by Panda et al. [42], which identified the same region downstream of the end of the potential core as the strongest sound producing source for high subsonic and supersonic single stream jets.

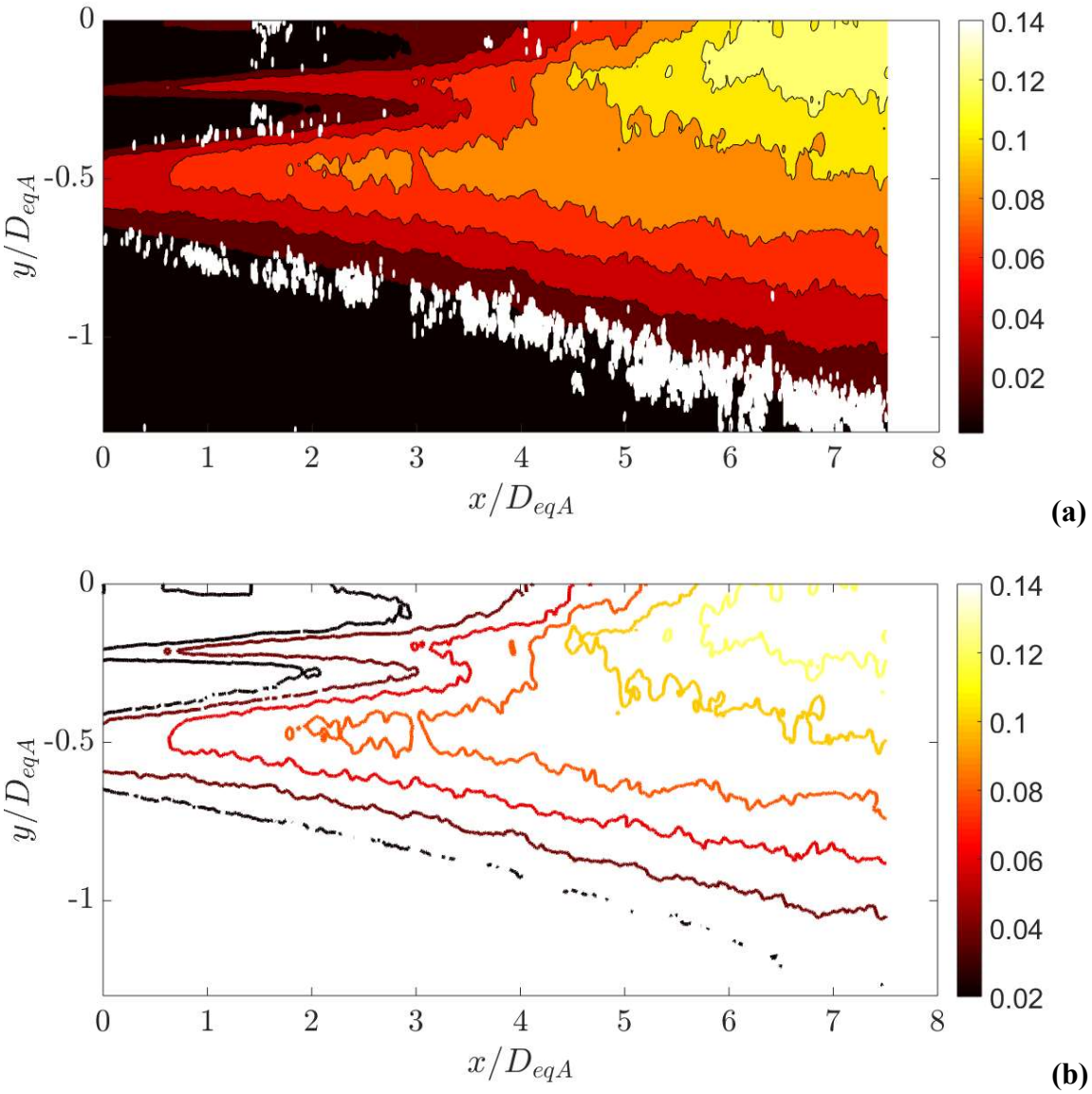

Figure 5.5. Axisymmetric case (a) NASA PIV turbulence intensity, u'/U_j in filled contour (b) NASA PIV turbulence intensity, u'/U_j in line contour plot

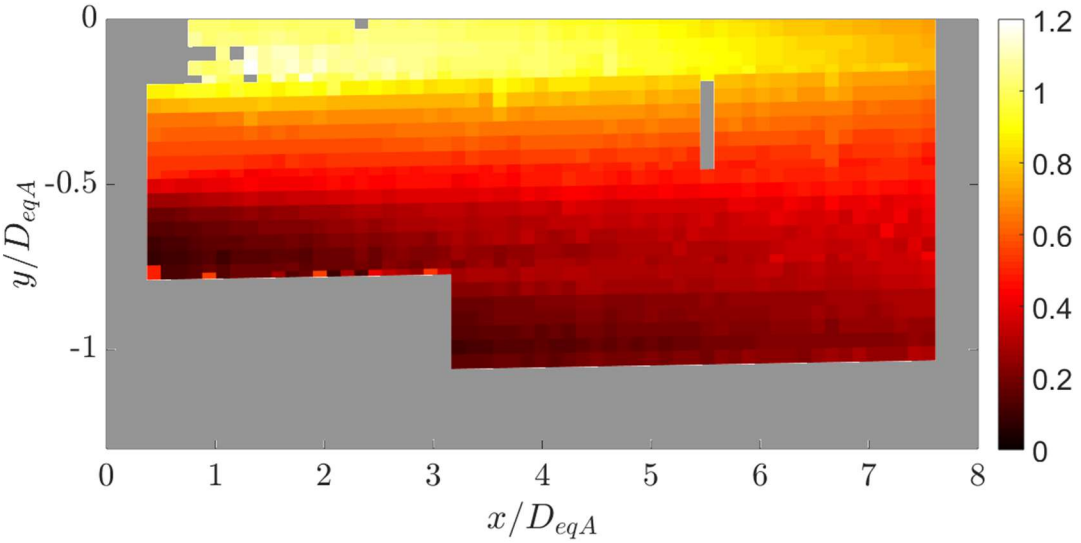

Figure 5.6. Axisymmetric case VT TR-DGV convection velocity, U_c/U_j

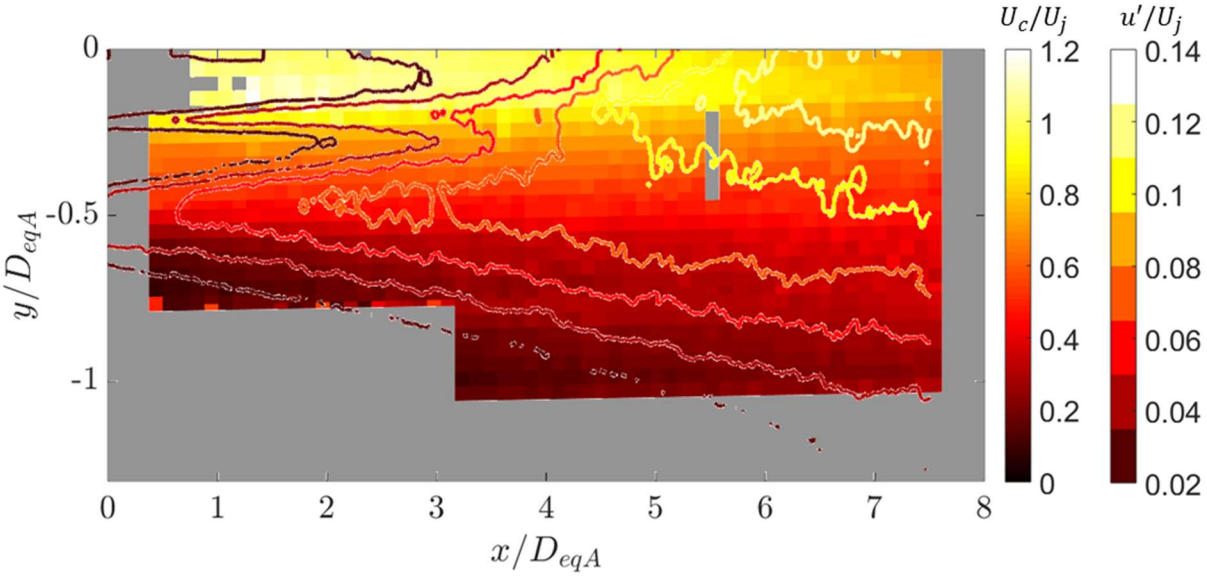

Figure 5.7. Overlaid contours of NASA PIV turbulence intensity, u'/U_j and VT TR-DGV convection velocity, U_c/U_j for the axisymmetric case. The background filled contour is the VT TR-DGV convection velocity and the overlaid line contour is the NASA PIV turbulence intensity

5.2. Offset Nozzle Configuration

In the following section only convection velocity results from the VT TR-DGV instrument are presented. For the offset nozzle configuration all results are for the locally "thicker" side of the jet. Comparison of the three stream axisymmetric nozzle convection velocity with that of the asymmetric offset case shown in Figure 5.8 reveals clear differences between the flow fields. The convection speeds at large radial locations are higher for the offset case. The increase in momentum due to the "thicker" shear layer is most likely responsible for this increase in convection velocity. Along the centerline, however, convection speeds for the offset configuration begin to decrease at an earlier axial location. This is evidence that offset causes the potential core to breakdown earlier compared to the axisymmetric configuration.

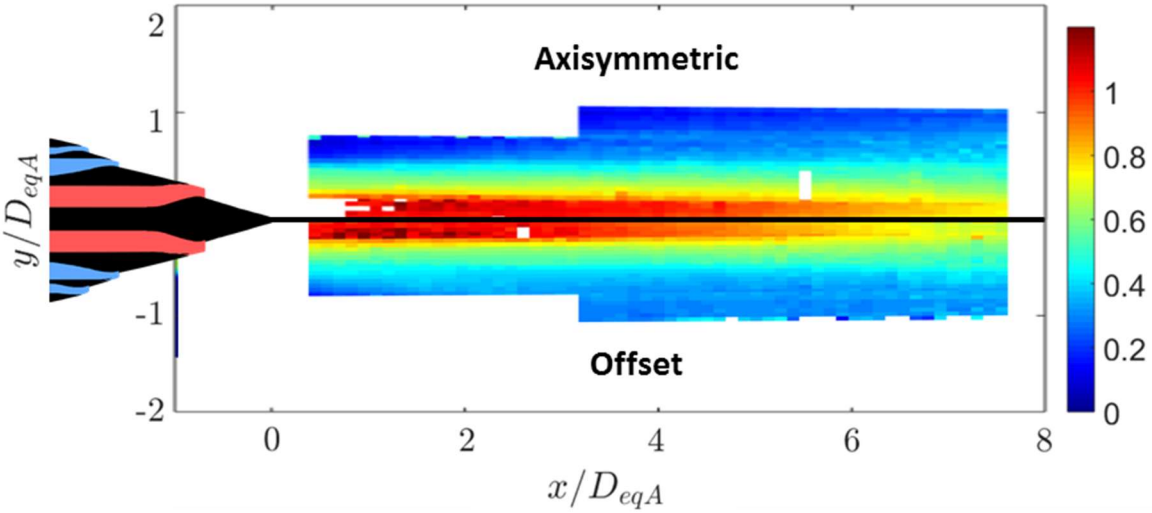

Figure 5.8. Comparison of convection velocity, U_c/U_j, (top) axisymmetric nozzle configuration and (bottom) offset nozzle configuration

The percent reduction/increase between the offset and axisymmetric case are shown in Figure 5.9. Positive values indicate an increase in convection velocities, while negative values indicate a reduction in convection velocities due to the offset configuration. The dotted black lines indicate the location of the potential cores for the core and bypass streams. Two regions are readily identified as reduction areas: one in the shear layer, and one along the centerline. The reduction in the shear layer region is expected as the introduction of a greater momentum stream will enhance the mixing and therefore entrainment of the ambient fluid to slow convection speeds. The regions

from x/D_{eqA} = 4 to 6 and slightly offset from the centerline around y/D_{eqA} = -0.1 which shows greatest reduction in convection velocities is in the vicinity of the end of the potential core. Specifically, the area around seven diameters downstream shows a reduction by almost 20%. Computational work by Papamoschou and Rostamimonjezi [6] and experimental work by Papamoschou and Phong [41] have also shown that noise reduction in asymmetric jets is in part caused by a reduction in the convection Mach number. Work by Veltin et al. [44] showed two areas of high correlation for jet noise, one before and one after the end of the potential core. It is likely that the two areas of reduction may be the two noise sources identified by Veltin et al. The introduction of the offset therefore reduces the noise generation in part through a reduction in the largest convection velocities both in the shear layer and along the centerline. It is important to note too that some regions in the flow have increased convection velocity, these are areas where the convection velocity is at most $0.2U_j$, and they would not impact the sound radiated to the far field, but rather may be important for energy dissipation as discussed next.

Recent computational work by Unnikrishnan and Gaitonde [66] suggests that vortex intrusion from the shear layer into the core is responsible for noise generation while entrainment of ambient fluid and the shear layer into the core causes dissipation as this shearing process dissipates energy. The net interaction of these two mechanisms show dissipation within the potential core while production in the shear layer and beyond the end of the potential core. As already discussed increased entrainment of the ambient fluid is observed in the offset configuration due to the higher convection speeds in the outer regions of the shear layer. A possible physical explanation of the noise reduction due to the offset, therefore, is the increased entrainment of the ambient air causes a stronger dissipation within in the core causing the potential core to collapse earlier. The earlier collapse reduces the convection velocity along the centerline earlier and overall causes the noise production region beyond the end of the potential core and in the shear layer to be reduced.

Additionally, the area along the centerline identified as having the greatest reduction in convection velocity for the offset case is the same area identified as having the highest convection velocities and turbulence intensity for the axisymmetric case in Figure 5.7. The reduction in convection velocity in this region may be partially responsible for the reduction in radiated noise on the “thick” side measured by Henderson et al [5]. It is also evident that the tertiary stream increases the convection velocity in the outer portion of the jet.

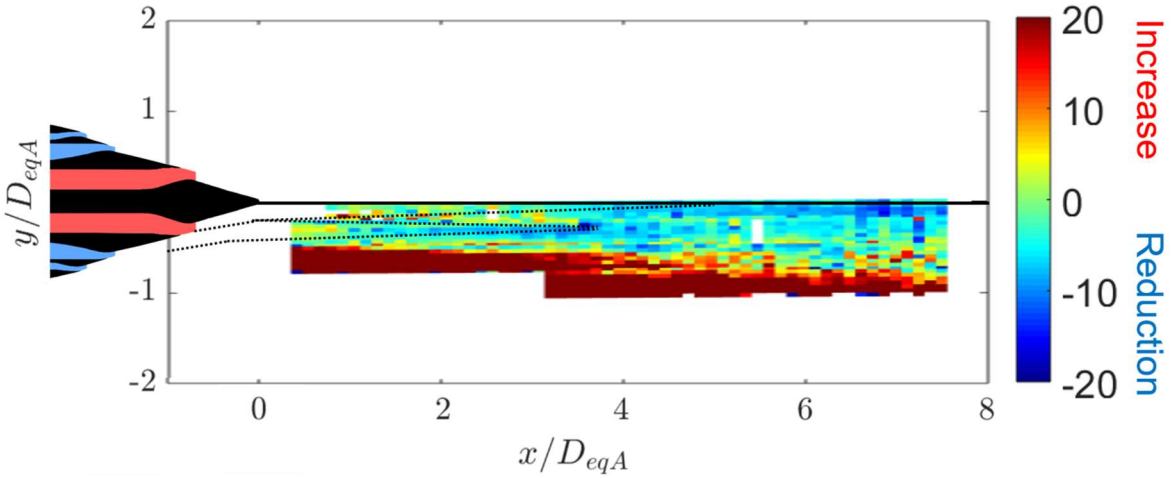

Figure 5.9. Contour of the percent difference between convection velocity, U_c, of the axisymmetric and offset three stream cases. Negative values indicate locations where the offset configuration reduces the U_c and positive values indication locations where the offset configuration increases U_c. The dotted black lines indicate the potential core region.

5.3. Wavepacket Model

The wavepacket model was applied to understand the effect of the observed convection velocities on radiated noise. The constant convection speeds used in the model of $0.6U_j$ and $0.8U_j$ came from the key reduction areas identified in the previous section for the axisymmetric configuration, while the constant convection speeds of $0.56U_j$ and $0.67U_j$ came from the offset configuration. Figure 5.10 and Figure 5.11 show the location of the convection velocities in reference to the axisymmetric nozzle configuration and offset nozzle configuration, respectively. The lower convection velocity case of $0.6U_j$ and $0.56U_j$ are characteristic convection velocities seen in the shear layer, while the higher convection velocity of $0.8U_j$ and $0.67U_j$ are observed in the region just in potential core breakdown region.

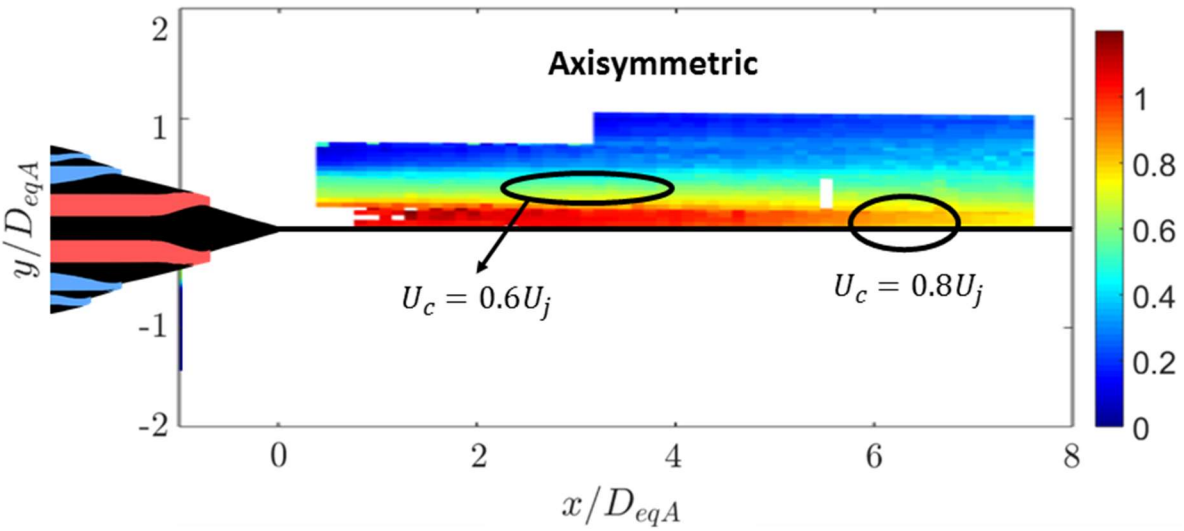

Figure 5.10. Location of regions identified for analysis of convection speed on radiated noise for axisymmetric

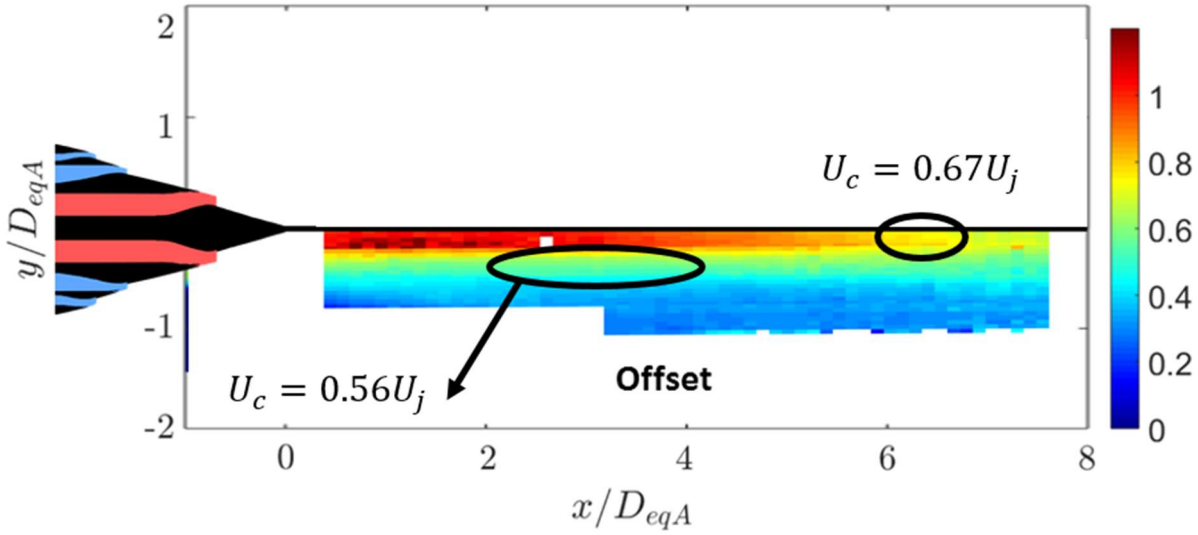

Figure 5.11. Location of regions identified for analysis of convection speed on radiated noise for offset configuration

From the wavepacket model, a wavenumber spectrum was calculated. The wavenumber spectra for a Strouhal number of 0.4 are shown in Figure 5.12. The red vertical line on the plots denotes the wavenumber found using the ambient speed of sound and the frequency based on the Strouhal number. Wavenumbers below the red line, in the shaded region, are the components that will radiate to the far field. The area under the wavenumber spectrum can be used as an

approximation for the energy contained in the wavepacket. Again, some kind of windowing function would have to applied to the wavenumber spectra to take it from kinetic energy to acoustic energy. As this windowing function is not known, the current wavenumber spectra will be analyzed and the shaded regions are considered the regions that have the highest potential to radiate energy. As can be seen in Figure 5.12, the wavepackets with a higher convection velocity radiates a greater proportion of its energy to the far as expected. Decreasing the convection velocity of the wavepacket tends to shift the wavenumber spectra to higher wavenumbers which then causes a lower proportion of the wavenumber components to radiate to the far field. Since a wavenumber is measure of spatial frequency, a shift to higher wavenumbers would manifest itself as structures with smaller characteristic lengths.

Even through structures in jets have been observed to have almost constant convection speeds, in the region in the vicinity of the breakdown of the potential core, an interaction of wavepackets with the higher speed flow in the potential core could result in convection speeds of $0.8U_j$. Although this type of interaction of one dimensional wavepackets has not yet been studied, but some experimental evidence and analystical model development has been done based on the hypothesis of higher order wavepacket modes interacting to produce the lower order modes [67]. A hypothesis is proposed that the breakdown of orderly, larger structures to smaller structures as observed by Kastner and Samimy [38] may be caused by the interaction of slower moving wavepackets from the shear layer with faster speed flow in the potential core. This interaction would result in faster moving wavepackets which radiate more energy to the far field. This mechanism may be responsible for the strong correlations along the centerline observed by Panda et al. [42]. As shown in Figure 5.9 the offset stream reduces the convection velocity along the centerline in the region around the potential core breakdown. The offset stream, therefore, seems to cause shear layer wavepackets to interact at an earlier axially location thus reducing the potential core and reducing the convection velocities earlier. The earlier reduction of convection speeds provides an explanation for the noise reduction observed due to the offset configuration.

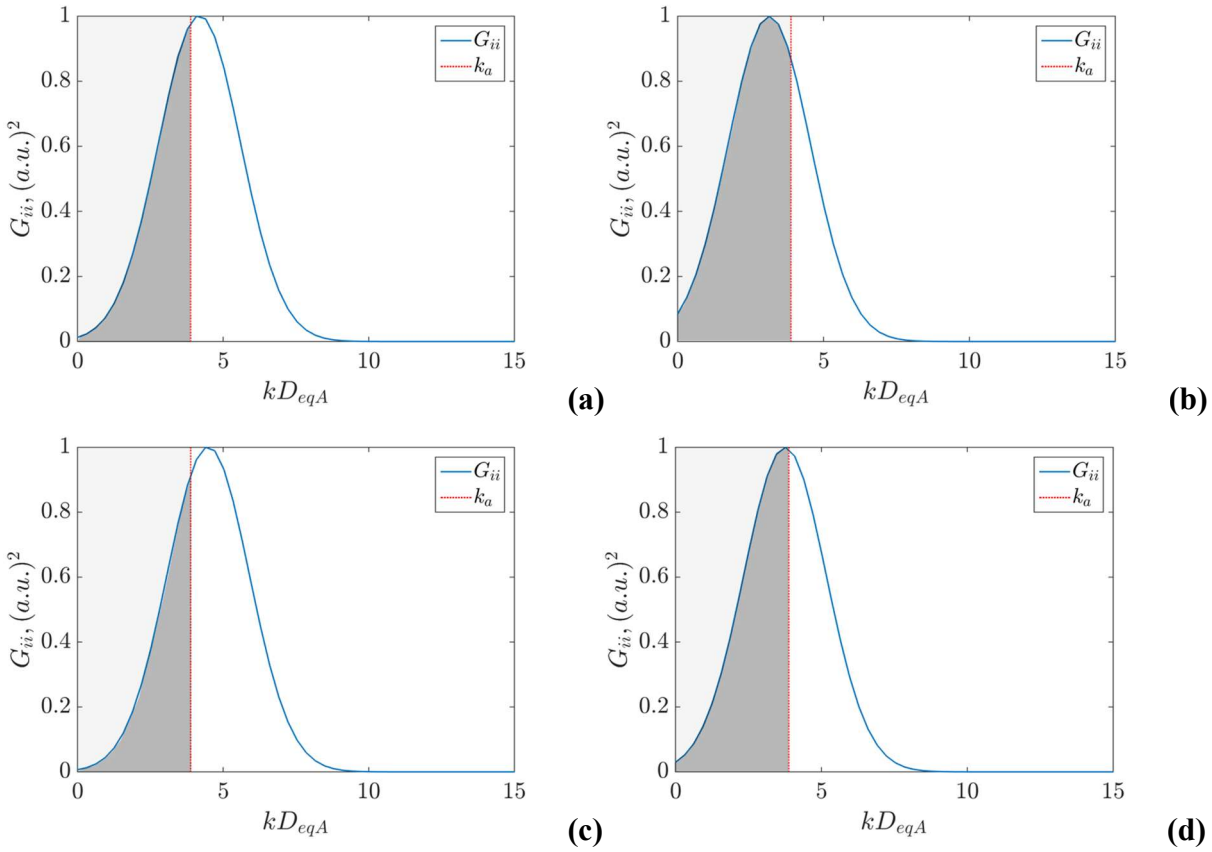

Figure 5.12. Wavenumber spectra for (a) $U_c = 0.6U_j$, (b) $U_c = 0.8U_j$, (c) $U_c = 0.56U_j$, and (d) $U_c = 0.67U_j$. Plots (a) and (b) are for the areas from the axisymmetric configuration, while (c) and (d) are from the offset configuration. Plots (a) and (c) are the areas in the shear layer, while (b) and (d) are areas near the centerline downstream of the potential core

Figure 5.13 shows the amount of energy that is likely to radiate at each Strouhal number for all the convection velocities studied. The likely energy to radiate is calculated by taking the ratio of the wavenumber spectrum integrated up to the red line, to the total integrated area of the wavenumber spectrum. For the higher convection velocity cases, representative of the centerline region, increasing the Strouhal number produces an increase in radiated energy. This is not the case for the lower convection velocity cases. For the lower convection velocity wavepackets representative of the shear layer region, the energy that is likely to radiate reaches a peak around a Strouhal number of 0.2. It is clear that at lower convection velocities the mid frequencies are more acoustically efficient, while the higher frequencies are more acoustically efficient in the higher convection velocity case. Overall, the difference between the axisymmetric and offset

configurations is greatest in the centerline region. In determining the mechanism responsible for noise reduction in nozzles with induced asymmetry is seems likely that the reduction in convection velocity near the centerline beyond the end of the potential core is the most significant contributor to noise reduction, sincde the reduction in energy likely to radiate is greatest for the centerline region.

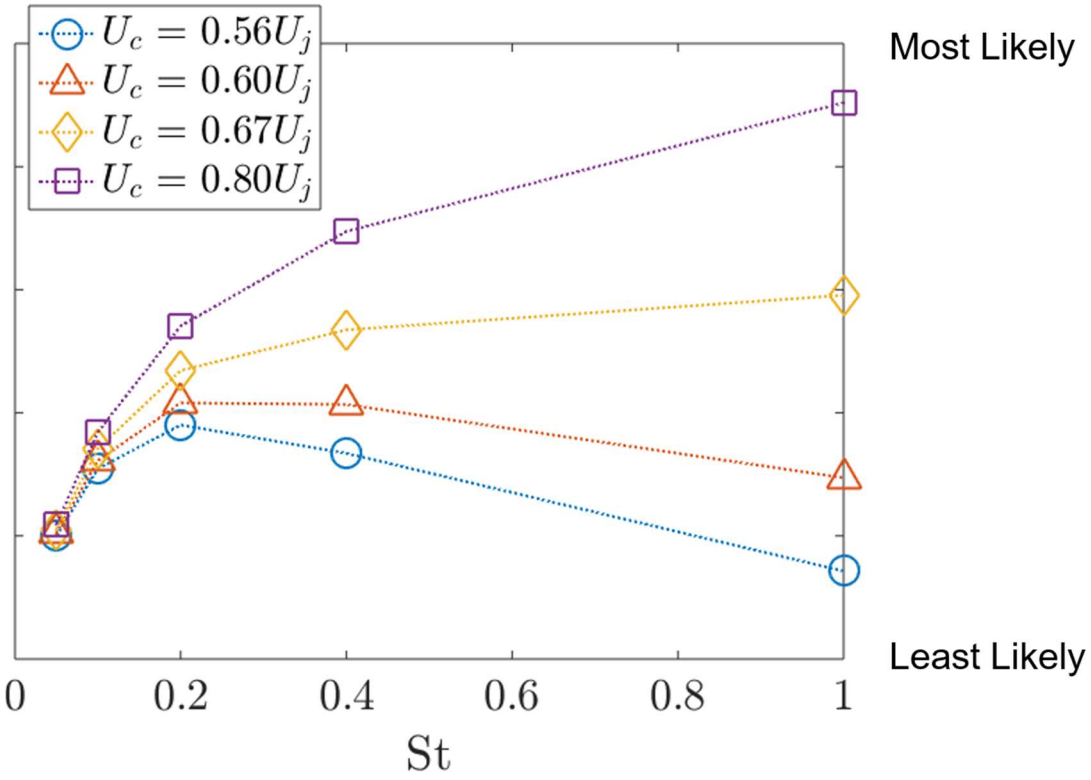

Figure 5.13. Comparison of amount of energy at each Strouhal number most likely to radiate for each convection velocitv studied

6. Conclusions

Noise sources were investigated for heated, three-stream nozzle configurations. Both an axisymmetric and an offset nozzle configuration were tested. Mean Velocity and turbulence intensity were provided from PIV measurements made by NASA. Convection velocity was measured using the VT TR-DGV instrument. The TTR for the core was 3.0 and for the bypass and tertiary streams was 1.25. The NPR for the core and bypass streams was 1.8, and the NPR for the tertiary stream was 1.4. Multichannel PMT detectors collected scattered laser light from particles injected in the flow. Simultaneous measurements from 32 channels of the PMT detector allowed

for calculation of the convection velocity of the particles using a statistical cross-correlation on the seeding signal along the four pixels in the axial direction. The convection velocity is the slope of the line of the points times of maximum correlation values plotted against axial spacing.

For the axisymmetric nozzle configuration, comparison of the VT TR-DGV convection velocity to the NASA PIV mean velocity measurements show the convection velocity lags the mean velocity along the centerline. Comparison of the VT TR-DGV convection velocity with turbulence intensity show the region along the centerline, from 4 to 6 nozzle diameters downstream have both high turbulence intensity and convection velocity. This finding is an indication that this region downstream of the end of the potential core may be an important region for noise generation. Further, comparison of the axisymmetric and offset convection velocity revealed in addition to the shear layer region, the same region along the centerline as the area of greatest reduction in convection velocity. These reductions in convection velocity offer explanation to reduction in noise on the "thick" side of the offset observed in acoustic measurements. The wavepacket model analysis showed the shift to higher wavenumbers with increasing convection velocity. Due to the greater shift in the wavenumber spectra in the centerline region, it is hypothesized that the reduction area along the centerline is more important for noise reduction compared to the shear layer region. In addition, higher frequencies are more acoustically efficient for higher convection velocities, while mid frequencies are more acoustically efficient for lower convection speeds. A hypothesis is proposed that the interaction of wavepackets in the shear layer on either side of the jet with potential core results in noise generation through an increase in convection speed of the interacting wavepackets from the value in the shear layer, typically around $0.6U_j$ to higher values around $0.8U_j$ as seen in the VT TR-DGV convection velocity data.

6.1. Recommendations for Future Work

To continue the current work of this thesis there are several additional data sets that would be beneficial: instantaneous flow data and pressure measurements. Additional data that may be available from the PIV data collected at NASA Glenn. From the PIV data, instantaneous velocity vectors can be obtained from which structures can be identified. The instantaneous velocity vectors are necessary to identify structures instead of the mean velocity since the flow most likely never takes the form of the mean velocity field. Various analysis can be done from the instantaneous velocity fields. First, flow structures can be identified by eye from the images. This approach will

provide evidence quickly as to whether or not the structures and interactions hypothesized in this thesis occur. Provided enough data is available, more robust approaches for structure identification such as conditional averaging and Proper Orthogonal Decomposition (POD) could be used. POD is a method that identifies structures in the flow by reconstructing the most probable realizations of the flow based on the input data [68]. The realizations are called modes, and the lowest mode contains the most energy and is the most probable realization of the flow. Analyzing the lowest modes would reveal the structures that are most probable in the flow. Comparing these flow structures to those hypothesized in this thesis and looking for evidence of the flow structures interacting with the potential core will provide insight into the nature of the noise sources in jets.

From the pressure data, the wavenumber/frequency spectra can be obtained. Comparison of the wavenumber frequency spectrum with those of a wavepacket model will help to improve the wavepacket model. The wavenumber/frequency spectra from pressure measurements will also provide evidence into how well the wavepacket model reproduces the radiating/non-radiating components of noise. In addition obtaining a true wavenumber/frequency spectra will also validate if using the convection velocity on the convective ridge is appropriate for the wavepacket model. Measuring the pressure in both the near field and far field will offer the ability to make comparisons. If a wavenumber/frequency spectra is obtained for both the far field and compared to the near field then the radiating/non-radiating components can be compared.

Coupling a flow structure identification analysis with pressure measurements will provide additional insight into both wavepackets and noise sources. Coupling POD analysis with near-field pressure measurements, as was done by Picard and Delville [65], could also provide additional evidence to support the existence of wavepacket like structures in jets. As it would be difficult to obtain near field pressure measurements at the same time as seed based velocity measurements in heated, high speed jets, other forms of structure identification may be necessary. Flow visualization using techniques such as Schlieren or Shadowgraphs may be sufficient to link structures in the flow with near field pressure measurements. A final analysis that would more closely link structures to noise would be to collect far field pressure measurements simultaneously with flow visualization. Flow visualization data could come from any of the above mentioned methods. Identification of these structures and tracking their features before and after sound is emitted as was done by Kastner et. al [38] will provided further proof of what is happening in the jet. Once the types of structures that emit sound are identified, methods can be developed to remove

or reduce the number of these structures/events that occur in the jet to meet the ultimate goal of noise reduction.

References

[1] G. M. Lilley, "The radiated noise from isotropic turbulence and heated jets," *Theor. Comput. Fluid Dyn.*, vol. 6, no. 5–6, pp. 281–301, 1994.

[2] D. L. Huff, B. S. Henderson, J. J. Berton, and J. A. Seidel, "Perceived Noise Analysis for Offset Jets Applied to Commercial Supersonic Aircraft," in *54th AIAA Aerospace Sciences Meeting*, San Diego, CA, 2016, pp. 1–12.

[3] B. Henderson, "Aeroacoustics of Three-Stream Jets," in *18th AIAA/CEAS Aeroacoustics Conference (33rd AIAA Aeroacoustics Conference)*, Colorado Springs, CO, 2012, pp. 5–6.

[4] D. Papamoschou, A. D. Johnson, and V. Phong, "Aeroacoustics of Three-Stream High-Speed Jets from Coaxial and Asymmetric Nozzles," *J. Propuls. Power*, vol. 30, no. 4, pp. 1055–1069, 2014.

[5] B. Henderson, S. J. Leib, and M. P. Wernet, "Measurements and predictions of the noise from three-stream jets," in *21st AIAA/CEAS Aeroacoustics Conference*, Dallas, TX, 2015.

[6] D. Papamoschou and S. Rostamimonjezi, "Modeling of Noise Reduction for Turbulent Jets with Induced Asymmetry," in *18th AIAA/CEAS Aeroacoustics Conference (33rd AIAA Aeroacoustics Conference)*, Colorado Springs, CO, 2012, pp. 4–6.

[7] V. F. Dippold, L. E. Foster, and M. R. Wiese, "Computational Analyses of Offset-Stream Nozzles for Noise Reduction," *J. Propuls. Power*, vol. 25, no. 1, pp. 204–217, 2009.

[8] NARC, "Report on Jet Engine Noise Reduction," *Nav. Res. Advis. Comm.*, no. April, 2009.

[9] S. Keefe, "F/A-18 Program Explores the Use of Exhaust Nozzle Chevrons to Reduce Engine Noise," *Currents: The Navy's Energy & Environmental Magazine*, pp. 6–19, 2015.

[10] D. Papamoschou, J. Xiong, and F. Liu, "Reduction of Radiation Efficiency in High-Speed Jets," in *20th AIAA/CEAS Aeroacoustics Conference*, Atlanta, GA, 2014, pp. 1–17.

[11] T. Ecker, K. T. Lowe, and W. F. Ng, "Scale-up of the Time-Resolved Doppler Global Velocimetry Technique," in *54th AIAA Aerospace Sciences Meeting*, San Diego, CA, 2016, pp. 1–13.

[12] D. G. Crighton, "Basic principles of aerodynamic noise generation," *Prog. Aerosp. Sci.*, vol. 16, no. 1, pp. 31–96, 1975.

[13] J. C. Lau, P. J. Morris, and M. J. Fisher, "Measurements in subsonic and supersonic free jets using a laser velocimeter," *J. Fluid Mech.*, vol. 93, no. 1, pp. 1–27, 1979.

[14] J. Bridges and M. Wernet, “Measurements of the Aeroacoustic Sound Source in Hot Jets,” in *9th Aeroacoustics Conference and Exhibit*, Hilton Head, SC, 2003, pp. 1–16.

[15] G. L. Brown and A. Roshko, “On density effects and large structure in turbulent mixing layers,” *J. Fluid Mech.*, vol. 64, no. 4, pp. 775–816, 1974.

[16] J. A. Schetz and R. D. W. Bowersox, *Boundary Layer Analysis*, 2nd ed. Reston, Virginia: American Institute of Aeronautics and Astronautics, 2011.

[17] C. E. Tinney and P. Jordan, “The near pressure field of co-axial subsonic jets,” *J. Fluid Mech.*, vol. 611, pp. 175–204, 2008.

[18] P. Jordan and T. Colonius, “Wave Packets and Turbulent Jet Noise,” *Annu. Rev. Fluid Mech.*, vol. 45, pp. 173–195, 2013.

[19] C. K. Tam, “Supersonic jet noise,” *Annu. Rev. Fluid Mech.*, vol. 27, no. 1, pp. 17–43, 1995.

[20] P. J. Morris and K. Viswanathan, “Jet Noise,” in *Noise Sources in Turbulent Shear Flows: Fundamental and Applications*, Vol. 525., R. Camussi, Ed. Springer Science & Business Media, 2013, pp. 119–196.

[21] S. B. Pope, *Turbulent Flows*. Cambridge: Cambridge University Press, 2000.

[22] M. J. Lighthill, “On sound generated aerodynamically I. General theory,” *Proc. R. Soc. London, Ser. A Math. Phys. Eng. Sci.*, vol. 211, no. 1107, pp. 564–587, 1952.

[23] M. J. Lighthill, “On Sound Generated Aerodynamically. II. Turbulence as a Source of Sound,” *Proc. R. Soc. London, Ser. A Math. Phys. Eng. Sci.*, vol. 222, no. 1148, pp. 1–32, 1954.

[24] J. E. Ffowcs-Williams, “The Noise from Turbulence Convected at High Speed,” *Philos. Trans. R. Soc. London*, vol. 255, no. 1061, pp. 469–503, 1963.

[25] H. S. Ribner, “Quadrupole correlations governing the pattern of jet noise,” *J. Fluid Mech.*, vol. 38, no. 1, p. 1, 1969.

[26] M. E. Goldstein and W. L. Howes, “New aspects of subsonic aerodynamic noise theory,” *NASA Tech. Note*, no. NASA TN D-7158, pp. 1–41, 1973.

[27] J. E. Ffowcs-Williams and G. Maidanik, “The Mach wave field radiated by supersonic turbulent shear flows,” *J. Fluid Mech.*, vol. 21, no. 4, pp. 641–657, 1965.

[28] C. Bailly, C. De Lyon, and P. Lafon, “Subsonic and Supersonic Jet Noise Predictions from Statistical Source Models,” *AIAA J.*, vol. 35, no. 11, pp. 1688–1686, 1997.

[29] Y. Du and P. J. Morris, “The separation of radiating and non-radiating near-field pressure

fluctuations in supersonic jets," *J. Sound Vib.*, vol. 355, pp. 172–187, 2015.

[30] E. Mollo-Christensen, "Jet noise and shear flow instability seen from an experimenter's viewpoint.," *J. Appl. Mech.*, pp. 1–7, 1967.

[31] D. Papamoschou and A. Roshko, "The compressible turbulent shear layer: an experimental study," *J. Fluid Mech.*, vol. 197, no. 1, p. 453, 1988.

[32] D. K. Mclaughlin, G. L. Morrison, and T. R. Troutt, "Experiments on the instability waves in a supersonic jet and their acoustic radiation," *J. Fluid Mech.*, vol. 69, no. 1, pp. 73–95, 1975.

[33] C. K. W. Tam and P. J. Morris, "The radiation of sound by the instability waves of a compressible plane turbulent shear layer," *J. Fluid Mech.*, vol. 98, no. 2, pp. 349–381, 1980.

[34] C. K. W. Tam, M. Golebiowski, and J. M. Seiner, "On the two components of turbulent mixing noise from supersonic jets," in *2nd AIAA/CEAS Aeroacoustics Conference*, State College, PA, 1996, pp. 1–18.

[35] P. J. Morris, "A note on noise generation by large scale turbulent structures in subsonic and supersonic jets," *Int. J. Aeroacoustics*, vol. 8, no. 4, pp. 301–315, 2009.

[36] D. G. Crighton and P. Huerre, "Shear-layer pressure fluctuations and superdirective acoustic sources," *J. Fluid Mech.*, vol. 220, pp. 355–368, 1990.

[37] C. K. W. Tam and D. E. Burton, "Sound generated by instability waves of supersonic flows. Part 1. Two-dimensional mixing layers," *J. Fluid Mech.*, vol. 138, pp. 249–271, 1984.

[38] J. Kastner, M. Samimy, J. Hileman, and J. B. Freund, "Comparison of Noise Mechanisms in High and Low Reynolds Number High-Speed Jets," *AIAA J.*, vol. 44, no. 10, pp. 2251–2258, 2006.

[39] D. Papamoschou, "Mach wave elimination in supersonic jets," *AIAA J.*, vol. 35, no. 10, pp. 1604–1611, 1997.

[40] B. S. Henderson and M. Wernet, "Characterization of Three-Stream Jet Flow Fields," in *54th AIAA Aerospace Sciences Meeting*, San Diego, CA, 2016, pp. 1–21.

[41] D. Papamoschou and V. C. Phong, "The Very Near Pressure Field of Single- and Multi-Stream Jets," in *55th AIAA Aerospace Sciences Meeting*, Grapevine, TX, 2017, pp. 1–16.

[42] J. Panda, R. G. Seasholtz, and K. A. Elam, "Investigation of noise sources in high-speed jets via correlation measurements," *J. Fluid Mech.*, vol. 537, pp. 349–385, 2005.

[43] J. I. Hileman, B. S. Thurow, E. J. Caraballo, and M. Samimy, "Large-scale structure

evolution and sound emission in high-speed jets: real-time visualization with simultaneous acoustic measurements," *J. Fluid Mech.*, vol. 544, pp. 277–307, 2005.

[44] J. Veltin, B. J. Day, and D. K. McLaughlin, "Correlation of Flow and Acoustic Field Measurements in High Speed Jets," *AIAA J.*, vol. 49, no. January, pp. 150–163, 2011.

[45] D. Papamoschou, P. J. Morris, and D. K. McLaughlin, "Beamformed Flow-Acoustic Correlations in a Supersonic Jet," *AIAA J.*, vol. 48, no. 10, pp. 2445–2453, 2010.

[46] P. O. A. L. Davies, M. J. Fisher, and M. J. Barratt, "The chracteristics of the turbulence in the mixing region of a round jet," *J. Fluid Mech.*, vol. 15, no. 3, pp. 337–367, 1962.

[47] J. C. Lau, M. J. Fisher, and H. . Fuchs, "The intrinsic structure of turbulent jets," *J. Sound Vib.*, vol. 22, no. 4, pp. 379–406, 1972.

[48] P. J. Morris and K. B. M. Q. Zaman, "Velocity measurements in jets with application to noise source modeling," *J. Sound Vib.*, vol. 329, no. 4, pp. 394–414, 2010.

[49] R. D. W. Bowersox, "Combined laser Doppler velocimetry and cross-wire anemometry analysis for supersonic turbulent flow," *AIAA J.*, vol. 34, no. 11, pp. 2269–2275, 1996.

[50] T. R. Troutt and D. K. McLaughlin, "Experiments on the flow and acoustic properties of a moderate-Reynolds-number supersonic jet," *J. Fluid Mech.*, vol. 116, no. 1, pp. 123–156, 1982.

[51] A. J. Smits and K. C. Muck, "Constant Temperature Hot-Wire anemomenter Practice in Supersonic Flows," *Exp. Fluids*, vol. 2, pp. 33–41, 1984.

[52] M. J. Doty and D. K. McLaughlin, "Space-time correlation measurements of high-speed axisymmetric jets using optical deflectometry," *Exp. Fluids*, vol. 38, pp. 415–425, 2005.

[53] B. P. Petitjean, K. Viswanathan, D. K. McLaughlin, and P. J. Morris, "Space-Time Correlation Measurements in Subsonic and Supersonic Jets Using Optical Deflectometry," in *13th AIAA/CEAS Aeroacoustics Conference (28th AIAA Aeroacoustics Conference)*, Rome, Italy, 2007, pp. 1–20.

[54] F. Kerhervé, P. Jordan, Y. Gervais, J. C. Valière, and P. Braud, "Two-point laser Doppler velocimetry measurements in a Mach 1.2 cold supersonic jet for statistical aeroacoustic source model," *Exp. Fluids*, vol. 37, pp. 419–437, 2004.

[55] J. C. Lau, "Laser velocimeter correlation measurements in subsonic and supersonic jets," *J. Sound Vib.*, vol. 70, no. 1, pp. 85–101, 1980.

[56] E. Murakami and D. Papamoschou, "Eddy Convection in Coaxial Supersonic Jets," *AIAA*

J., vol. 38, no. 4, pp. 628–635, 2000.

[57] J. Bridges, "Effect of Heat on Space-Time Correlations in Jets," in *12th AIAA/CEAS Aeroacoustics Conference (27th AIAA Aeroacoustics Conference)*, Cambridge, MA, 2006, pp. 1–16.

[58] T. Ecker, K. T. Lowe, and W. F. Ng, "Eddy Convection in Developing Heated Supersonic Jets," *AIAA J.*, vol. 53, no. 11, pp. 3305–3315, 2015.

[59] T. Ecker, K. T. Lowe, and W. F. Ng, "On the Distribution and Scaling of Convective Wavespeeds in the Shear Layers of Heated Supersonic Jets," *Flow, Turbul. Combust.*, 2016.

[60] B. S. Thurow, N. Jiang, J. H. Kim, W. Lempert, and M. Samimy, "Issues with measurements of the convective velocity of large-scale structures in the compressible shear layer of a free jet," *Phys. Fluids*, vol. 20, no. 6, 2008.

[61] T. Ecker, D. R. Brooks, K. T. Lowe, and W. F. Ng, "Development and application of a point Doppler velocimeter featuring two-beam multiplexing for time-resolved measurements of high-speed flow," *Exp. Fluids*, vol. 55, no. 9, pp. 1–15, 2014.

[62] J. H. Wernet and M. P. Wernet, "Stabilized Alumina/Ethanol Colloidal Dispersion for Seeding High Temperature Air Flows," in *Proceedings of the ASME Symposium on Laser Anemometry: Advances and Applications*, Lake Tahoe, NV, 1994.

[63] M. J. Fisher and P. O. A. L. Davies, "Correlation measurements in a non-frozen pattern of turbulence," *J. Fluid Mech.*, vol. 18, no. 1, pp. 97–116, 1964.

[64] D. Papamoschou, "Wavepacket Modeling of the Jet Noise Source," in *17th AIAA/CEAS Aeroacoustics Conference (32nd AIAA Aeroacoustics Conference)*, Portland, OR, 2011, pp. 1–20.

[65] C. Picard and J. Delville, "Pressure velocity coupling in a subsonic round jet," *Int. J. Heat Fluid Flow*, vol. 21, no. 3, pp. 359–364, 2000.

[66] S. Unnikrishnan and D. V. Gaitonde, "Acoustic mode and sources in a supersonic jet," in *55th AIAA Aerospace Sciences Meeting*, Grapevine, TX, 2017, pp. 1–13.

[67] X. Wu and P. Huerre, "Low-frequency sound radiated by a nonlinearly modulated wavepacket of helical modes on a subsonic circular jet," *J. Fluid Mech.*, vol. 637, p. 173, 2009.

[68] C. Tropea, A. L. Yarin, and J. F. Foss, Eds., *Springer Handbook of Experimental Fluid Mechanics*. Berlin, Heidelberg: Springer Berlin Heidelberg, 2007.

A. Appendix

A.1. Calibration

Due to the difficulty of the instrument set-up, the convection velocity results were calibrated using the NASA PIV mean velocity data. The sensor spacing was updated based on anchoring the convection velocity results with the NASA PIV mean velocity. As shown in Figure A.1 the fifth point from the core was adjusted so that it was the same as the NASA PIV mean velocity. A change in sensor spacing is a simple multiplication factor that effects the values of the convection velocity. The resulting change in sensor spacing was an increase of 1.14 mm. This change in sensor size is considered acceptable as it is a small change in compared to the size of the test rig. The new sensor spacing was applied to all the locations and found to better match the expected trends of convection velocity in the potential core.

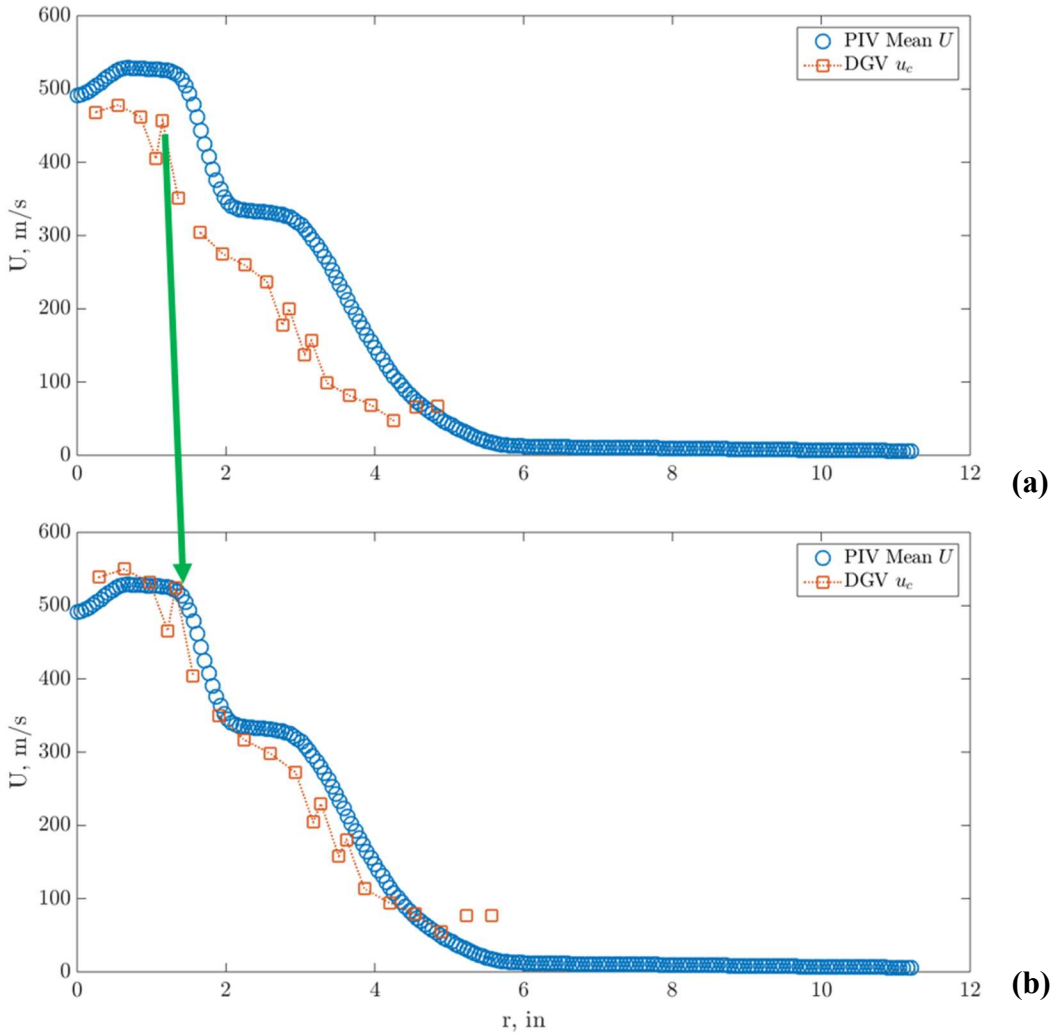

Figure A.1. Calibration of convection velocity using mean velocity (a) before calibration (b) after sensor spacing calibration. Green arrow indicates point used as anchor to find the new sensor spacing

In addition to the new sensor spacing, it was found that a radial offset between the overlapping measurement planes needed. An offset of 0.3" in the outward radial direction smoothed the radial profiles, giving a much more realistic radial profile. This correction is shown in Figure A.2. Again as this shift is small compared to the size of the testing rig this change is considered acceptable. This consistent radial shift was applied to all measurement planes and resulting in much smoother radial profiles along the entire length of the jet. The resulting radial profiles are given in the Section A.2.

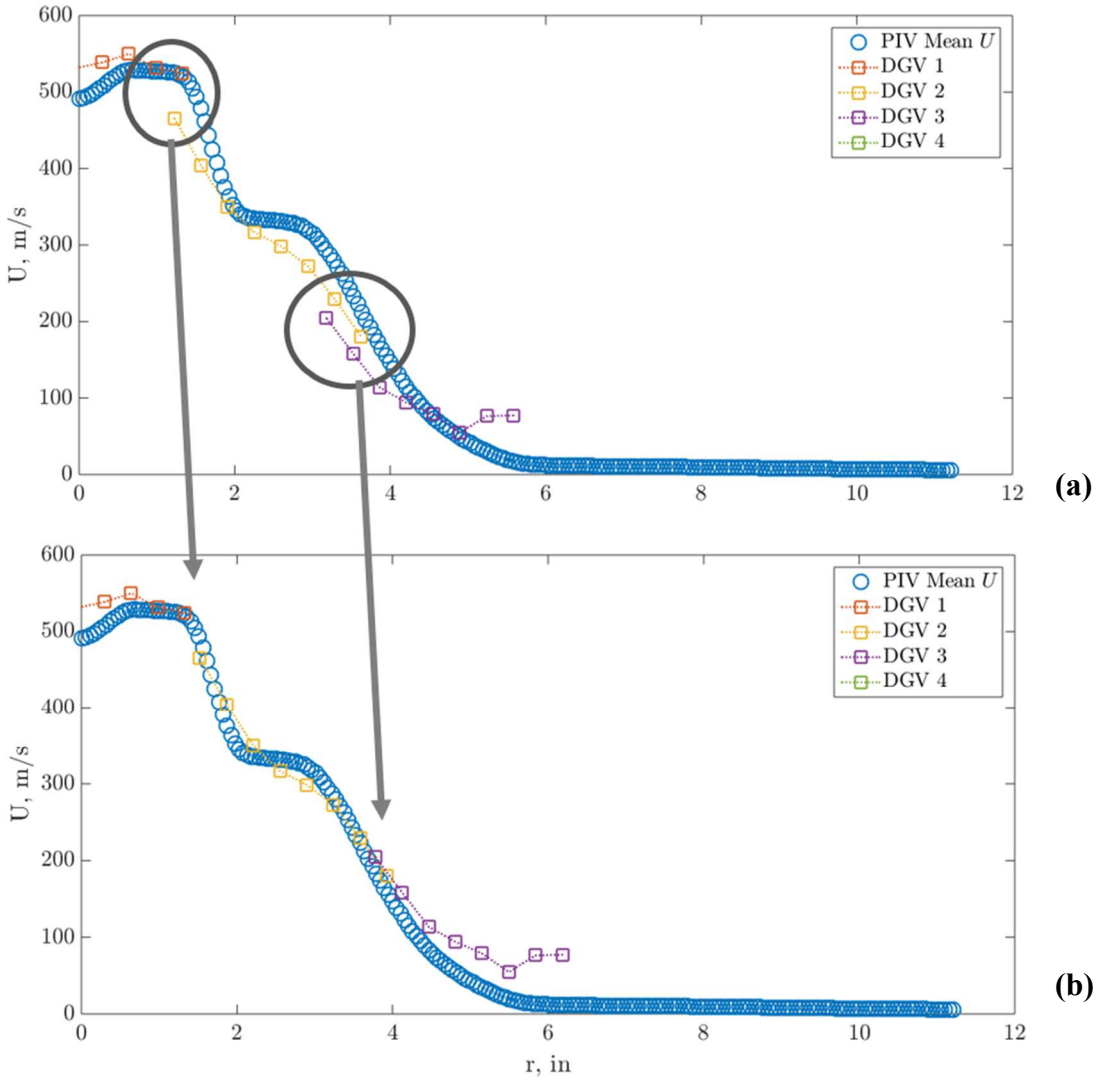

Figure A.2. Radial planes calibration of convection velocity (a) before radial offset (b) after radial offset calibration. Gray arrows show radial correction regions

A.2. Radial Profiles

Additional radial profiles are presented in Figure A.3. As the distance from the nozzle exit is increased the convection velocity in the shear layer becomes larger than the mean velocity.

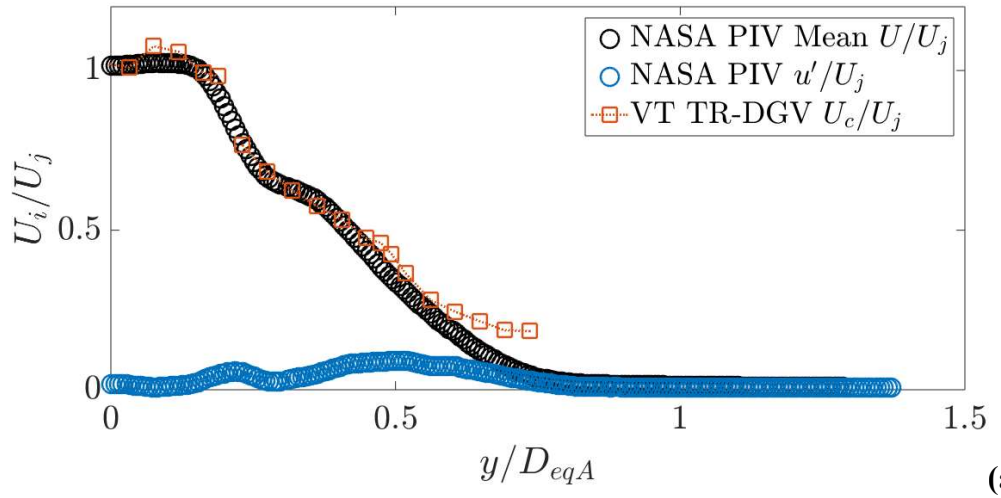

(a)

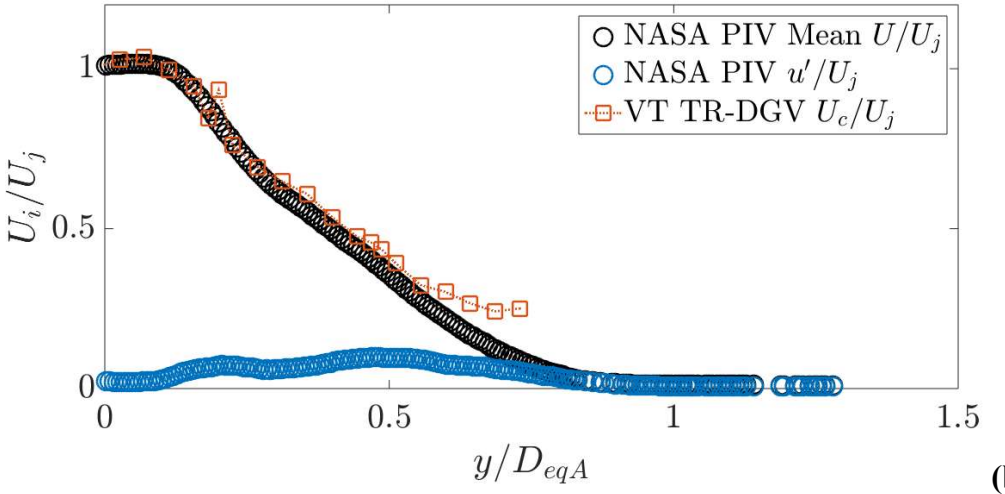

(b)

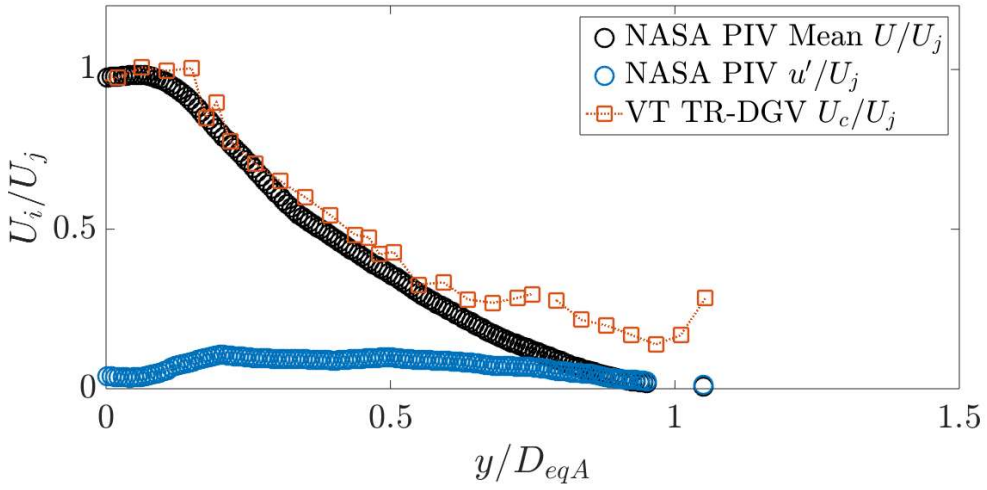

Figure A.3. Caption on next page

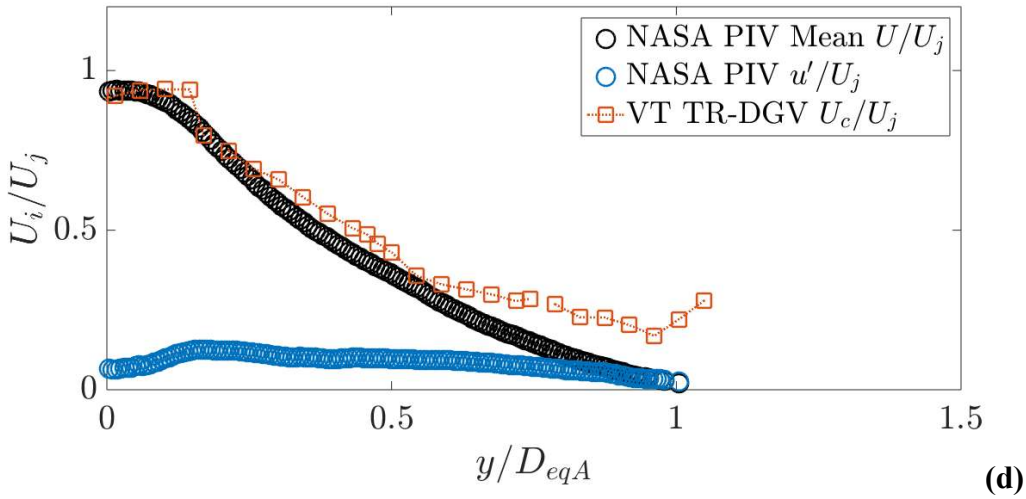

(d)

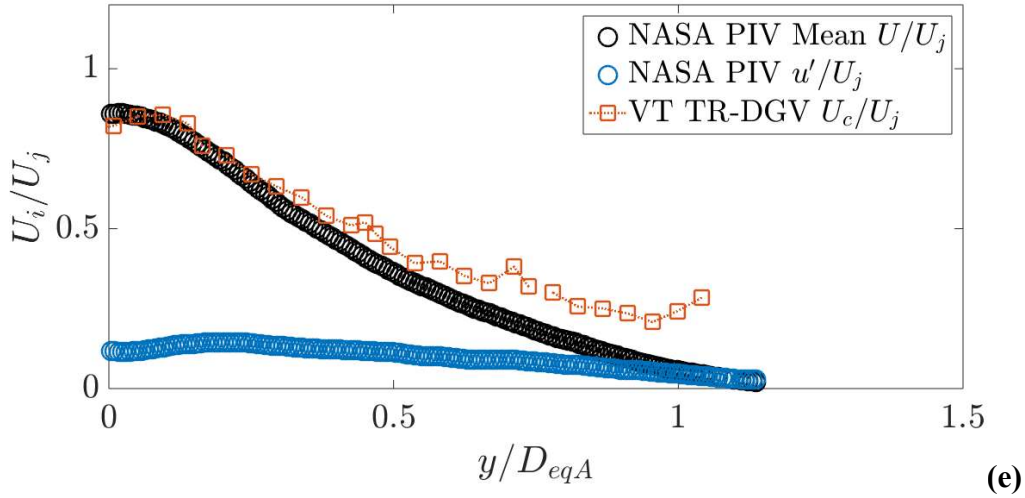

(e)

Figure A.3. Radial contours at (a) x/D_{eqA}=2.0, (b) x/D_{eqA}=3.0, (c) x/D_{eqA}=4.0, (d) x/D_{eqA}=5.0, and (e) x/D_{eqA}=6.0

A.3. Uncertainty Analysis

Ecker et al. [58] has shown that the total uncertainty of the convection velocity is a function of the uncertainty of the sensor spacing and the uncertainty of the lag time. The total uncertainty can be calculated using Equation (A.1).

$$\frac{\partial u_c}{u_c} = \sqrt{\left(\frac{\partial \Delta x}{\Delta x}\right)^2 + \left(\frac{\partial \tau}{\tau}\right)^2} \tag{A.1}$$

Based on the analysis of Ecker et al. [58] the uncertainty in the lag time was shown to be a function of the SNR and interpolation method used to find the maxima of the cross-correlation curves. It was shown that a cubic spline had the lowest uncertainty for all SNR, therefore, it was the interpolation method used in the calculation of convection velocity. The SNR of the seeding signal was approximated using Equation (A.2).

$$SNR \approx \sigma^2_{deterministic}/\sigma^2_{random} \tag{A.2}$$

The variance of the random content and the variance of the signal was approximated from the auto-correlation curves. The peak value at zero lag is the variance from both the random and deterministic components of the signal. The value of the auto-correlation curve at the next lag value to the right of zero was used as an approximation of the variance of the deterministic content. By subtracting the variance of the deterministic content from the total variance, the variance of the random part was approximated. Using the approximated values in Equation (A.2) gave an estimate of the SNR. Ecker et al. [58] provide a chart showing the effect of SNR on the uncertainty in the lag time. Based on the SNR calculated, the uncertainty in the lag time was found to be ±0.05.

The uncertainty in the sensor spacing was found by multiplying the uncertainty in the sensor spacing provided from the manufacturer sensor by the magnification of the optical setup. The resulting uncertainty in the sensor spacing was found to be ±0.05. Using Equation (A.1), the total uncertainty in the convection velocity calculation was found to be ±0.07. These results are summed up in Table A.1.

Table A.1. Uncertainty Parameters

$\partial \Delta x/\Delta x$	$\partial \tau/\tau$	$\delta U_c/U_c$
±0.05	±0.05	±0.07

A.4. Wavepacket Model

For the wavepacket model introduced Section 4.3 the radian frequencies used in Equation (4.2) were found using the Strouhal number. The Strouhal number is defined in Equation (A.3).

$$St = fD_{eqA}/U_j \tag{A.3}$$

Since the Strouhal number, diameter, and isentropic exit velocity are known, the frequency can be solved for then converted to radian frequency, ω, which is used in Equation (4.2) to define the waveform for the wavepacket model. The wavepacket shapes not presented in Section 4.3 are shown in Figure A.4 through Figure A.7.

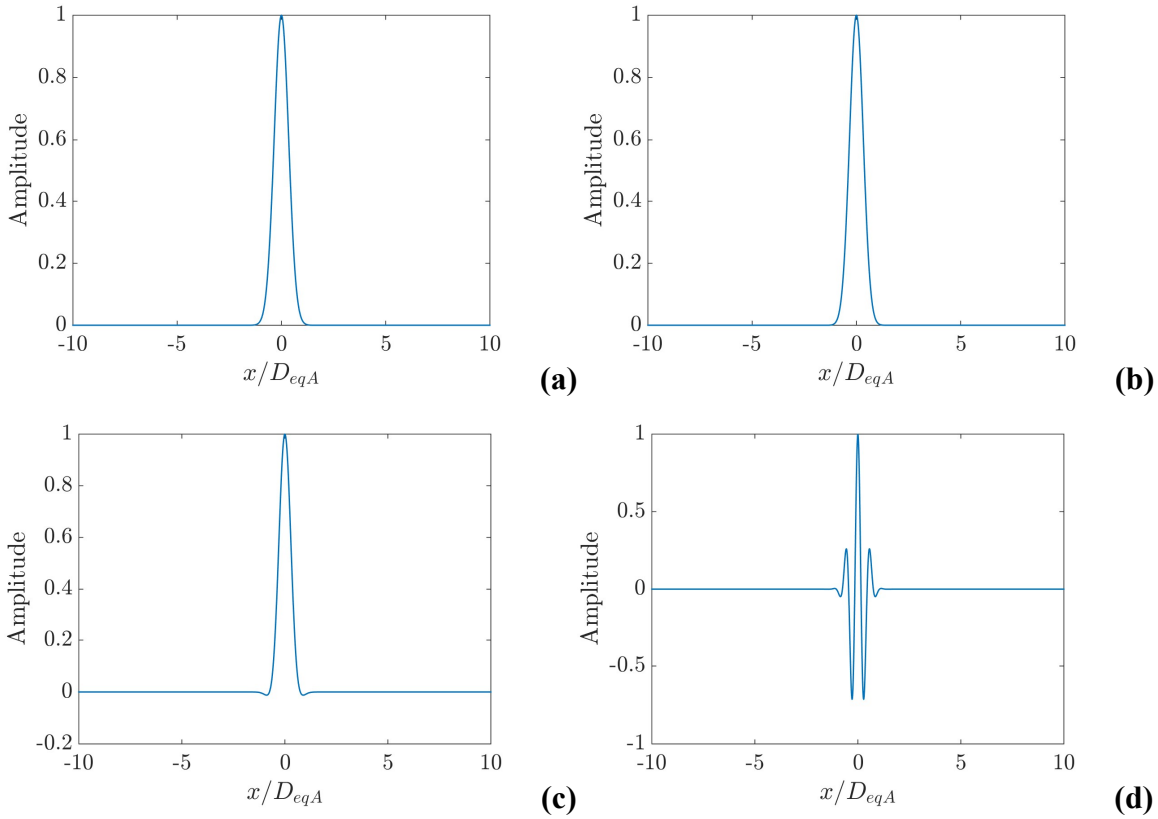

Figure A.4. Wave packet shapes for Convection Velocity case of $0.6U_j$ (a) St = 0.05, (b) St = 0.1, (c) St = 0.2, and (d) St = 1.0

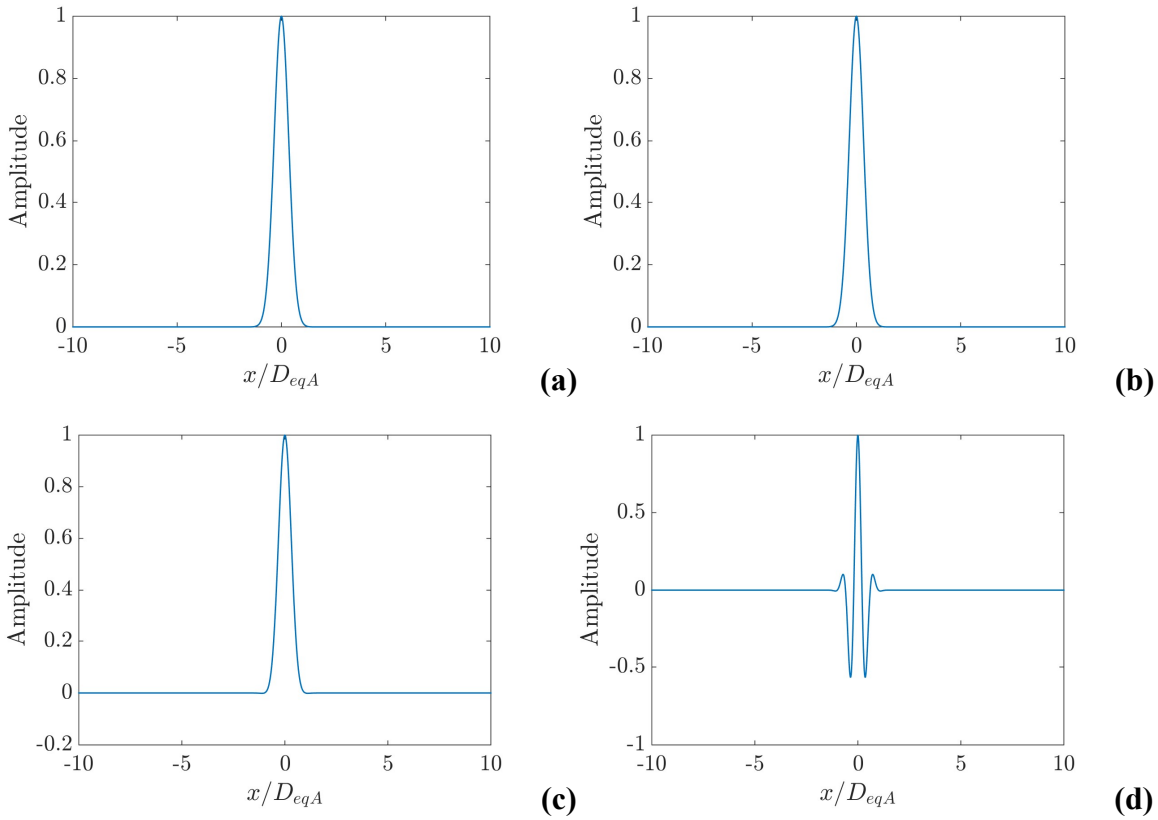

Figure A.5. Wave packet shapes for Convection Velocity case of $0.8U_j$ (a) St = 0.05, (b) St = 0.1, (c) St = 0.2, and (d) St = 1.0

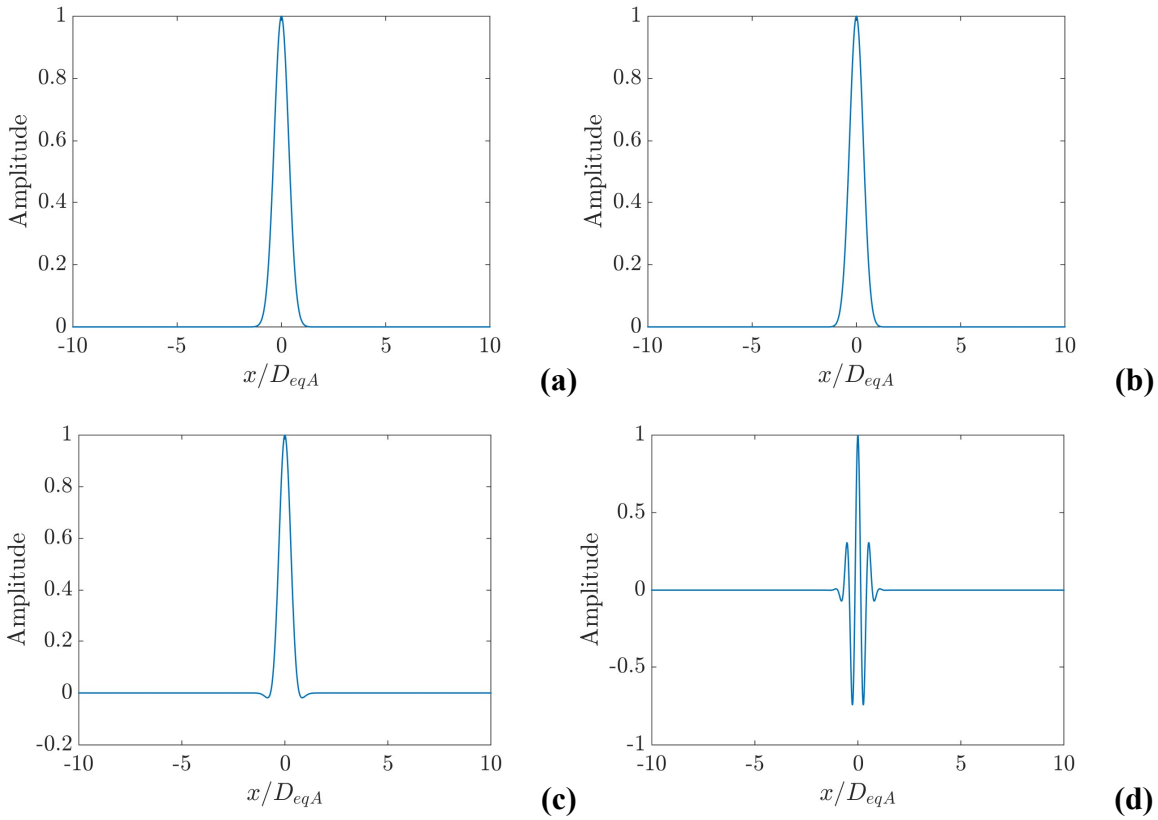

Figure A.6. Wave packet shapes for Convection Velocity case of $0.56U_j$ (a) St = 0.05, (b) St = 0.1, (c) St = 0.2, and (d) St = 1.0

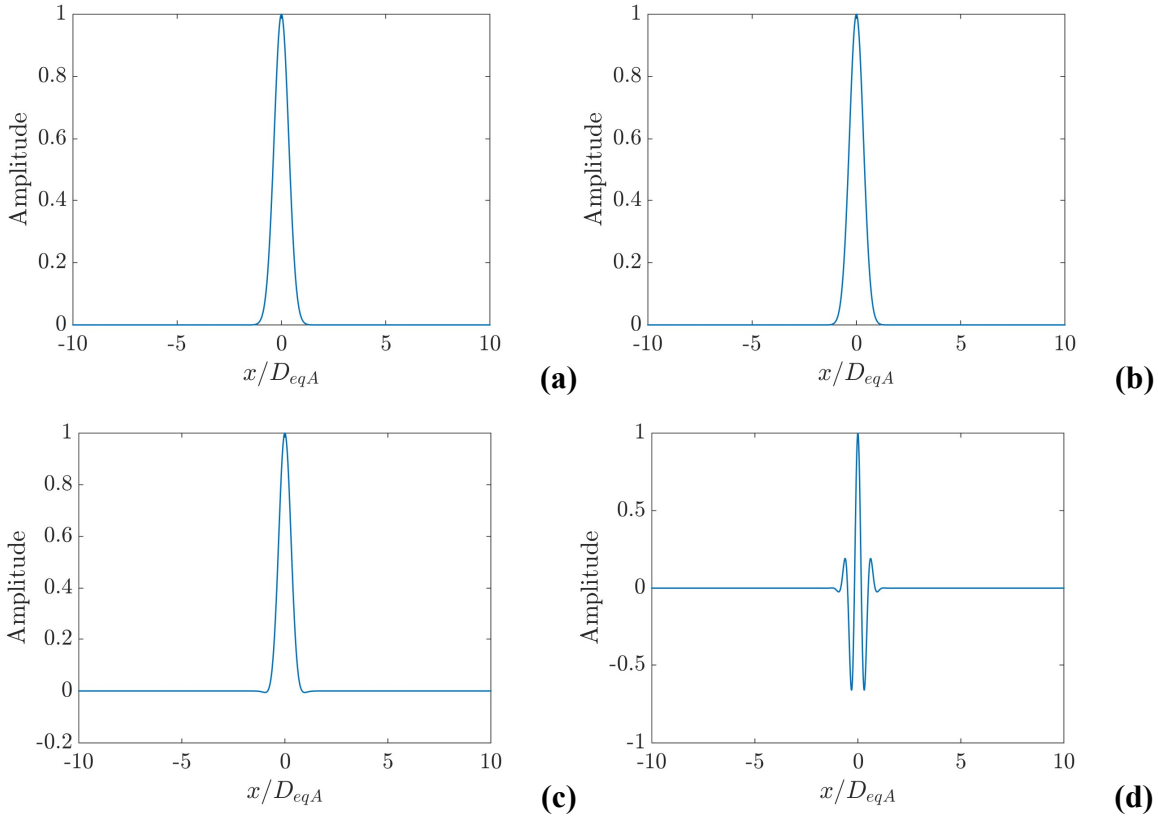

Figure A.7. Wave packet shapes for Convection Velocity case of $0.67U_j$ (a) St = 0.05, (b) St = 0.1, (c) St = 0.2, and (d) St = 1.0

Since the windowing function of the wavepacket was chosen as a Gaussian, the wavenumber spectrum can be calculated analytically shown in Equation (A.4).

$$G_{ii} = \frac{1}{\sqrt{2\pi}} e^{-(2\pi k - k_0)^2 l^2} \tag{A.4}$$

The integration of the wavenumber spectra was done numerically using a trapezoidal method. Wavenumber spectra not presented in Section 5.3 are shown in Figure A.8 through Figure A.11.

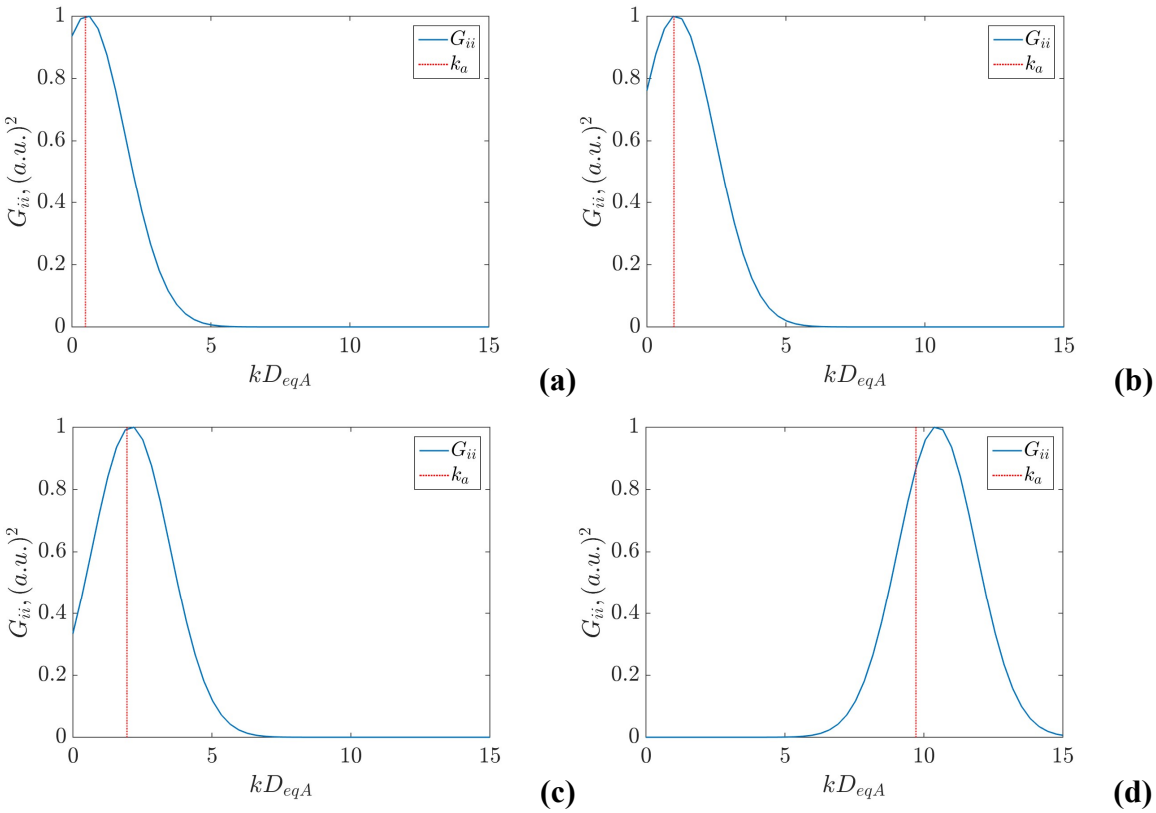

Figure A.8. Wavenumber spectra for Convection Velocity case of $0.6U_j$ (a) St = 0.05, (b) St = 0.1, (c) St = 0.2, and (d) St = 1.0

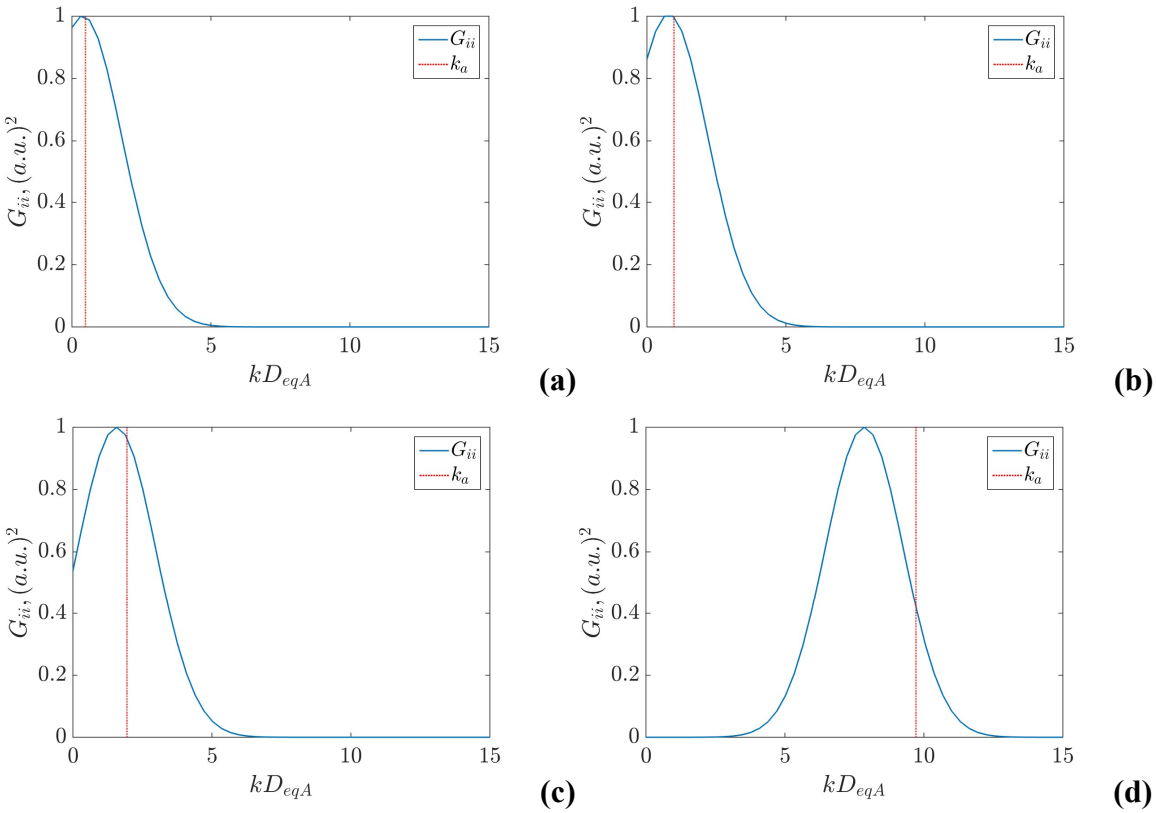

Figure A.9. Wavenumber spectra for Convection Velocity case of $0.8U_j$ (a) $St = 0.05$, (b) $St = 0.1$, (c) $St = 0.2$, and (d) $St = 1.0$

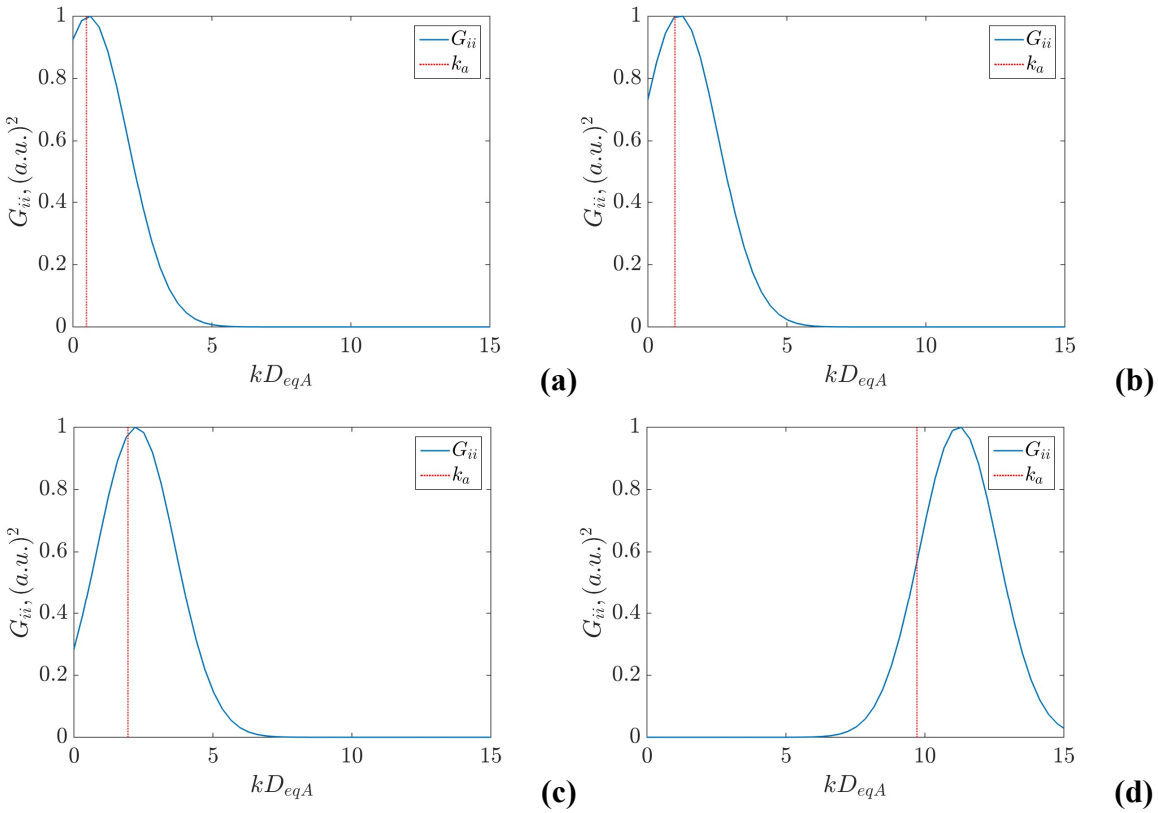

Figure A.10. Wavenumber spectra for Convection Velocity case of $0.56U_j$ (a) $St = 0.05$, (b) $St = 0.1$, (c) $St = 0.2$, and (d) $St = 1.0$

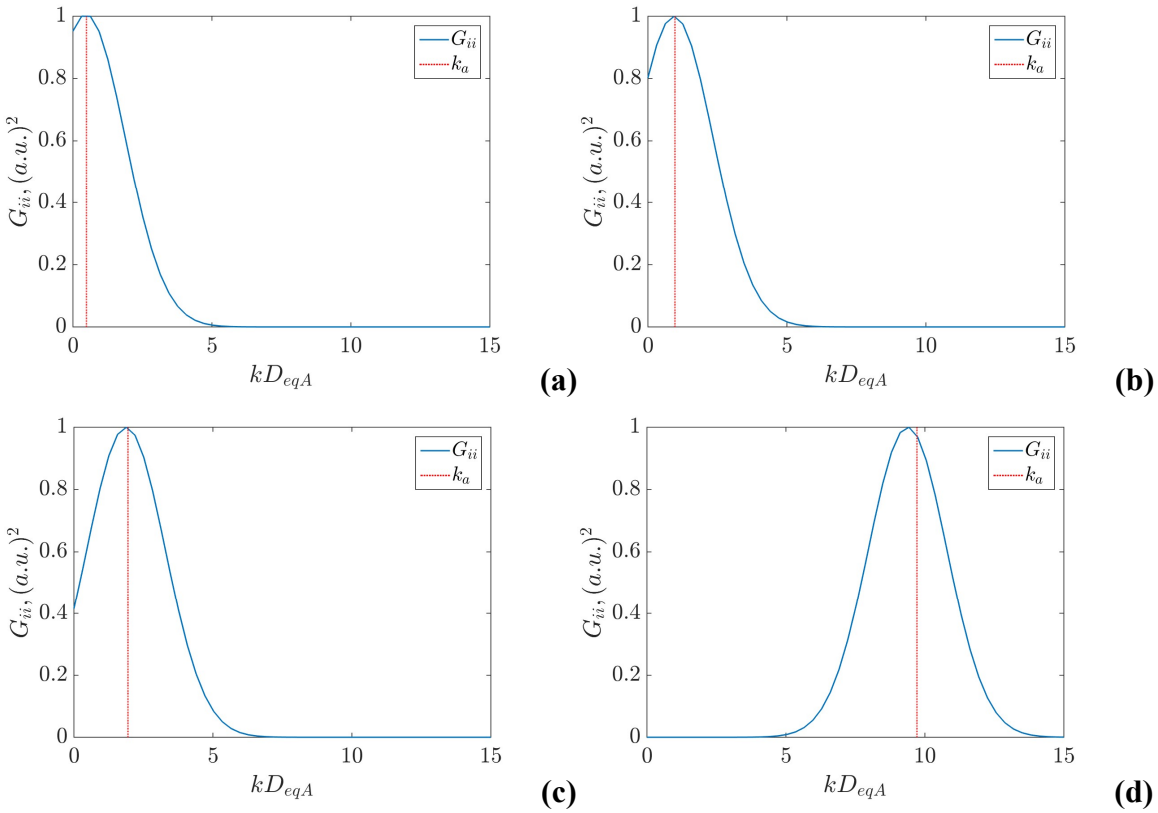

Figure A.11. Wavenumber spectra for Convection Velocity case of $0.67U_j$ (a) $St = 0.05$, (b) $St = 0.1$, (c) $St = 0.2$, and (d) $St = 1.0$

In addition the percentage of radiated energy shown in Figure 4.7. the total energy of two fo the wavepackets was analyzed as a function of Strouhal number, shown in Figure A.12. As can be seen, the integrated energy does not seem to be a function of convection velocity. Overall the higher frequency components have greater total energy. For the higher convection velocity case studied, since the higher frequency components were more acoustically efficient more energy will be radiated since the high frequency components are the high energy and acoustically efficient components. For the lower convection velocity case, the higher frequency components are not as acoustically efficient, therefore a lower proportion of the high energy components are radiating as noise.

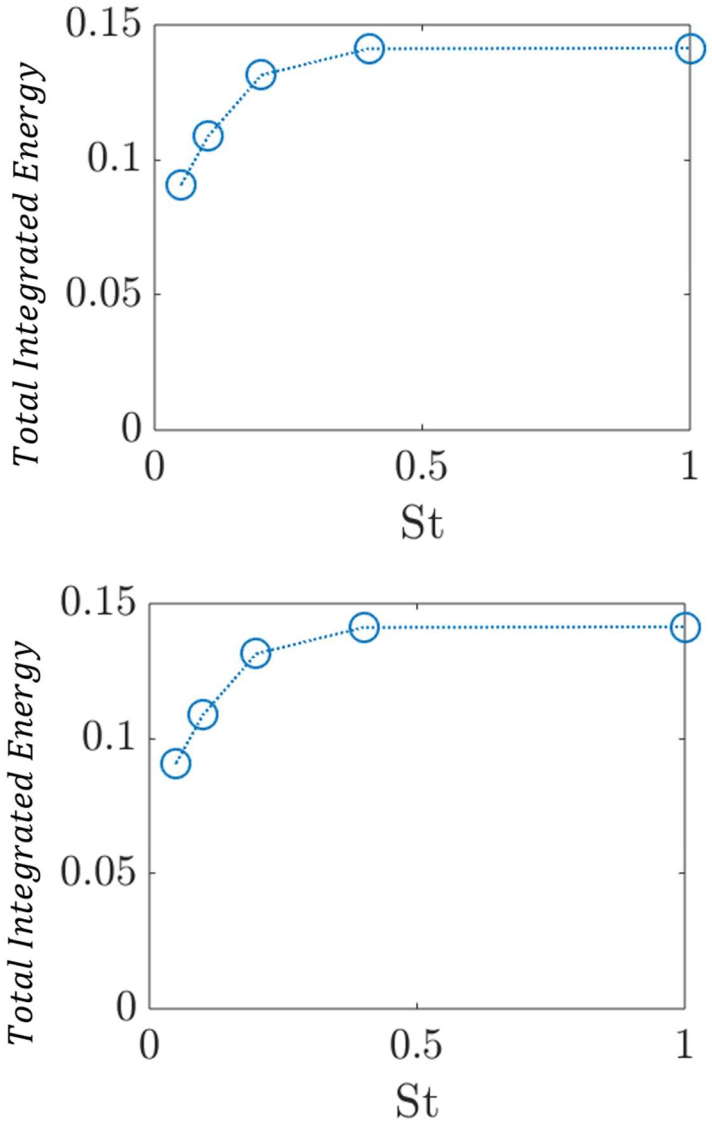

Figure A.12. Total integrated energy of the wavepacket as a function of Strouhal number for (a) $U_c = 0.6U_j$ and (b) $U_c = 0.8U_j$